

Classification of the quantum chaos in colored Sachdev-Ye-Kitaev models

Fadi Sun,^{1,2,4} Yu Yi-Xiang,³ Jinwu Ye,^{2,4} and Wu-Ming Liu^{3,5}

¹*Key Laboratory of Terahertz Optoelectronics, Ministry of Education, Department of Physics, Capital Normal University, Beijing 100048, China*

²*Department of Physics and Astronomy, Mississippi State University, Mississippi 39762, USA*

³*Beijing National Laboratory for Condensed Matter Physics, Institute of Physics, Chinese Academy of Sciences, Beijing 100190, China*

⁴*Kavli Institute of Theoretical Physics, University of California, Santa Barbara, Santa Barbara, California 93106, USA*

⁵*School of Physical Sciences, University of Chinese Academy of Sciences, Beijing 100190, China*



(Received 3 April 2019; published 8 January 2020)

The random matrix theory (RMT) can be used to classify both topological phases of matter and quantum chaos. We develop a systematic and transformative RMT to classify the quantum chaos in the colored Sachdev-Ye-Kitaev (SYK) model first introduced by Gross and Rosenhaus. Here we focus on the two-colored case and the four-colored case with a balanced number of Majorana fermions N . By identifying the maximal symmetries, the independent parity conservation sectors, the minimum (irreducible) Hilbert space, and especially the relevant antiunitary and unitary operators, we show that the color degrees of freedom lead to novel quantum chaotic behaviors. When N is odd, different symmetry operators need to be constructed to make the classifications complete. The two-colored case only shows the threefold Wigner-Dyson way, and the four-colored case shows the tenfold generalized Wigner-Dyson way which may also have nontrivial edge exponents. We also study two- and four-colored hybrid SYK models, which display many salient quantum chaotic features hidden in the corresponding pure SYK models. These features motivate us to develop a systematic RMT to study the energy level statistics of two or four uncorrelated random matrix ensembles. The exact diagonalizations are performed to study both the bulk energy level statistics and the edge exponents and to find excellent agreement with our exact maximal symmetry classifications. Our complete and systematic methods can be easily extended to study the generic imbalanced cases. They may be transferred to the classifications of colored tensor models, quantum chromodynamics with pairings across different colors, quantum black holes, and interacting symmetry protected (or enriched) topological phases.

DOI: [10.1103/PhysRevD.101.026009](https://doi.org/10.1103/PhysRevD.101.026009)

I. INTRODUCTION

The classification of phases of matter has a long history. It spans from the Landau theory on the classifications of all the possible spontaneous symmetry-breaking states to more recent classifications of the topological insulators and superconductors [1–3] of noninteracting electrons using the same symbols and techniques as the random matrix theory (RMT). The latter inspired and triggered the classifications of topological phases of interacting bosons or fermions which break no symmetries [3,4]. On the other forefront, there are recent extensive research activities on studying quantum chaos and quantum information scrambling in the Sachdev-Ye-Kitaev (SYK) model [5–9] and its various invariants. Because the ground states of SYK models are quantum spin liquids which neither break symmetry nor have any kind of topological order, one may need to classify the SYK models by a different organization pattern of matter which describes how quantum information is scrambled in the system: the quantum chaos.

There are two completely independent ways to characterize the quantum chaos. One way is to evaluate the out-of-time-ordered correlation (OTOC) functions to describe the quantum information scrambling at an early time (Ehrenfest time) [10–17]. It was found that the SYK models show the maximal quantum chaos, with the largest possible Lyapunov exponent $\lambda_L = 2\pi/\beta$ saturating the quantum chaos bound [18]. This salient feature ties that of quantum black holes, which are the fastest quantum information scramblers in nature. This fact suggests that the SYK model may be a boundary theory of some sort of bulk dilaton gravity theory such as the well-known Jackiw-Teitelboim (JT) gravity [19,20].

Another way is to use the RMT to describe the energy level statistics (ELS), which can be used to probe the late-time (Heisenberg time) dynamics [21–27]. It was found that the ELS of the Majorana fermion SYK can be described by the threefold-way Wigner-Dyson distributions in an $N \pmod{8}$ periodicity [22–24]. The RMT has also

been employed to study the quantum chaotic behaviors of event horizon fluctuations of black holes [23].

The quantum chaos in the SYK models is due to the quenched disorders. However, it inspired a new class of clean quantum mechanical models called colored (Gurau-Witten) or uncolored (Klebanov-Tarnopolsky) tensor models [28–33], which share similar quantum chaotic properties to the SYK, at least in the large- N limit [34]. Despite the lack of quenched disorders, the quantum chaos in tensor models seems much more difficult to analyze by either OTOC or RMT [33]. OTOC and RMT [35] may also be used to demonstrate the quantum chaos in a clean quantum optics model called the Dicke model, which describes the N qubits interacting with a single-photon mode with both rotating-wave and counter-rotating-wave interacting terms [36–39].

Gross and Rosenhaus [12] generalized the SYK model to a colored SYK, which contains $a = 1, 2, \dots, f$ colors; each has N_a sites with a q_a -body interaction. The model has a total number of Majorana particles, $N_t = \sum_{a=1}^f N_a$, and a total $q = \sum_{a=1}^f q_a$ -body interaction. It contains f towers of operators. The SYK model can be treated as the $f = 1$ special case with just one tower of operators. For the balanced case with $N_a = N_t/f$ and $q_a = q/f$, after the quenched disorder average is performed, the system has a reduced symmetry $O(N_t/f) \times O(N_t/f) \times \dots \times O(N_t/f)$, compared to the SYK model with $N_t = fN_a$ sites and $q = fq_a$ -body interaction, which has a full $O(N_t)$ symmetry. The operator spectrum contains a tower identical to that of SYK with a $q = fq_a$ -body interaction. The $h = 2$ operator, which is the lowest-dimensional operator in this tower, still leads to the maximal chaos. There is also a new tower of operators with degeneracy $f - 1$. The lowest-dimensional operator in this new tower is a $h = 1$ operator, whose operator product expansion (OPE) coefficient vanishes. There may be some intricate relations between the colored SYK and the colored tensor (Gurau-Witten) models [31,32]. Here, we study the quantum chaos in the colored SYK from the RMT, which would be complementary to the OTOC study by Gross and Rosenhaus [12]. For simplicity, we only focus on the balanced $q = 4$ cases with $f = 2$ and $f = 4$ colors. The analysis is much more involved, and the results are dramatically different from the Majorana or complex fermion SYK model. Our main results are presented in Tables III and IV, and in Figs. 2, 5, and 6.

The two-colored SYK only shows a threefold Wigner-Dyson way. For the cases where N is even, there are two conserved parities (Q_1, Q_2) corresponding to the two colors. We construct one antiunitary operator P which keeps the parities and commutes with the Hamiltonian. For $N \pmod{4} = 0$, the ELS is in the Gaussian orthogonal ensemble with a degeneracy $d = 1$ in a given parity sector (Q_1, Q_2) and total degeneracy $d_t = 1$ in the total parity sector $Q_t = Q_1 + Q_2$. For $N \pmod{4} = 2$, the ELS is in the Gaussian unitary ensemble with degeneracy $d = 1$ but total degeneracy $d_t = 2$. For the cases where N is odd, we add

two decoupled Majorana fermions with each color at infinity to construct Hilbert space separately for the two colors. So it still leads to two conserved parities (Q_1, Q_2) corresponding to the two colors. Adding two Majorana fermions into the system doubles the Hilbert space, but it also gives one more conserved parity. There is an additional antiunitary operator P_z , which also keeps the parities and commutes with the Hamiltonian and plays complementary roles to P . In both cases of $N \pmod{4} = 1, 3$, the ELS is in the Gaussian orthogonal ensemble with $d = 1$ in a given parity sector (Q_1, Q_2) . But P and P_z exchange their roles in the two cases, so $d_t = 1 + 1$ in the total parity sector $Q_t = Q_1 + Q_2$ in the twice-enlarged Hilbert space. Then exact diagonalizations are performed in the minimal Hilbert space, which matches our theoretical classification results (Fig. 2). We also study a hybrid two-colored SYK model which violates the (Q_1, Q_2) parities but conserves the total parity Q_t . It shows several novel quantum chaotic behaviors at all $N \pmod{4}$ values (Fig. 3), which are hidden in the pure two-colored SYK model. Our systematic approach can also be extended to a generic case with different N_a 's, $a = 1, 2$.

The four-colored case shows dramatically different quantum chaotic behaviors from the two-colored case. Due to a possible spectral mirror symmetry, the four-colored SYK is classified in a tenfold way, which may also show nontrivial hard-edge universality. For the four-colored case, there are always three independent conserved parities (Q_{12}, Q_{23}, Q_{34}) corresponding to the sums of two of the four colors. For the even- N case, the three independent conserved parities commute with each other. We construct one antiunitary operator P which keeps the parities and commutes with the Hamiltonian, and also find another antiunitary operator P_m which keeps the parities and anticommutes with the Hamiltonian. The product of the two antiunitary operators leads to a unitary chirality operator $\Lambda = PP_m$, which is nothing but the individual parity of each color, which anticommutes with the Hamiltonian. So when $N \pmod{4} = 0, 2$, the ELS is in the classes BDI and CI, respectively, with $d = 1$ in a given parity sector (Q_{12}, Q_{23}, Q_{34}) . In addition to the bulk RMT index $\beta = 1$, due to the chiral (mirror) symmetry, it also has the edge exponents $\alpha = 0, 1$, respectively. It is the chiral symmetry which dictates such a nontrivial ‘‘bulk-edge’’ correspondence. For the odd- N case, Q_{23}^0 does not commute with the other two parities anymore. So one only has two mutually conserved parities (Q_{12}^0, Q_{34}^0) . Then we add four decoupled Majorana fermions with each color at infinity to construct Hilbert space separately for the four colors. This enlarges the Hilbert space by 4 times, but it also leads to two more conserved parities. So the complete set of mutually commuting conserved parities becomes $(Q_{12}, Q_{23}, Q_{34}, Q_{0t})$ in the enlarged Hilbert space. The two antiunitary P, P_m and the chirality operator Λ still exist after shifting $N \rightarrow N + 1$, but P keeps the parities and P_m swaps each of the parities.

When $N \pmod{4} = 3, 1$, the ELS is in class AI in both cases with $d = 1$. We also identify another antiunitary operator P_z , which commutes with the Hamiltonian, but it swaps each parity in (Q_{12}, Q_{23}, Q_{34}) , thus keeping the same total parity $Q_t = Q_{12} + Q_{34}$ and Q_{0t} . This fact leads to $d_t = 2$ in the total parity (Q_t, Q_{0t}) when N is odd. Then exact diagonalizations are performed to confirm our theoretical results (Fig. 5), especially the edge exponent for $N \pmod{4} = 0, 2$ (Fig. 6). We also study a hybrid four-colored SYK model which violates the (Q_{12}, Q_{23}, Q_{34}) parities, but conserves the total parity (Q_t, Q_{0t}) . It shows several novel quantum chaotic behaviors at all $N \pmod{4}$ values (Fig. 3), which are hidden in the pure four-colored SYK model. Our systematic approach can also be extended to the imbalanced cases with different N_a 's, $a = 1, 2, 3, 4$. The broad impacts of the methods and results achieved in the paper and some perspectives are summarized in the concluding section.

As a byproduct, we develop a systematic RMT to study the energy level statistics of two or four uncorrelated random matrix ensembles. We then apply the new RMT to study several salient features of the two- or four-colored hybrid SYK models in Secs. IV and VI, respectively.

Finally, in the three appendixes, we discuss the intercolor representation, which is independent of whether N is odd or even, so it can be most conveniently used to perform our exact diagonalizations in the minimum Hilbert space. We perform our classifications on two- and four-colored SYK models and their corresponding hybrids in this minimum Hilbert space. To allow for comparisons to the results achieved with intracolor representations in the main text, when N is odd, we also add decoupled Majorana fermions at ∞ and perform our classifications in the enlarged Hilbert space. We reach the same conclusions among the three different classification schemes (namely, the two different intercolor schemes in the appendixes and the intracolor scheme in the main text), which may bring additional and considerable insights into the physical picture.

II. ENERGY LEVEL STATISTICS IN PURE AND MIXED RANDOM MATRIX THEORY

In this section, we first review the known results on the statistics of the nearest-neighbor (NN) energy level spacings initiated in Ref. [40] and the next-nearest-neighbor (NNN) energy level spacings initiated in Ref. [27] in pure random matrix ensembles. Then we generalize the NN and NNN statistics to the cases with mixed two and four uncorrelated and identically distributed (UCID) random matrix ensembles. The results will be heavily used in the following sections when discussing two-colored or four-colored hybrid SYK models.

A. The statistics of NN and NNN energy level spacings in pure random matrix ensembles

Let $\{e_n\}$ be an ordered set of eigenenergy obtained from the Hamiltonian; then the energy level spacing is

$s_n = e_{n+1} - e_n$, and the ratios of NN energy level spacings and NNN energy level spacings are defined as $r_n = s_{n+1}/s_n$ and $r'_n = (s_{n+3} + s_{n+2})/(s_{n+1} + s_n)$, respectively.

By considering a 2×2 matrix system, Wigner derived a simple approximate probability distribution function (Wigner surmise): $P_{w,\beta}(s) = a_\beta s^\beta e^{-b_\beta s^2}$, where $\beta = 1, 2, 4$ are the Dyson indices for the Gaussian orthogonal ensemble (GOE), the Gaussian unitary ensemble (GUE), and the Gaussian symplectic ensemble (GSE), respectively. The probability distribution function for independent random energy levels yields the Poisson distribution $P_p(s) = e^{-s}$. However, in order to compare different results from different systems, the energy levels will need an unfolding procedure, which is not convenient when large enough statistics are not available.

The NN ratio r and NNN ratio r' are introduced in Refs. [40] and [27], respectively, to overcome the difficulties in unfolding. Because taking the two ratios can get rid of the dependence on the local density of states, the unfolding becomes unnecessary. By considering a 3×3 matrix system, the authors in Ref. [40] obtained the Wigner-like surmises of the ratio of the NN level spacing distribution $P_w(r) = \frac{1}{Z_\beta} \frac{(r+r^2)^\beta}{(1+r+r^2)^{1+3\beta/2}}$, where $\beta = 1, 2, 4$ and $Z_\beta = 8/27, 4\pi/81\sqrt{3}$, and $4\pi/729\sqrt{3}$ for the GOE, GUE, and GSE, respectively. The Poisson result is $P_p(r) = \frac{1}{(1+r)^2}$. The distribution function $P_w(r)$ has the same level repulsion at small r as $P_w(s)$ —namely, $P_w(r) \sim r^\beta$. However, the large- r asymptotic behavior $P_w(r) \sim r^{-(2+\beta)}$ is dramatically different from the fast exponential decay of $P_w(s)$.

By considering a 5×5 matrix system, a Wigner-like surmise of the ratio of the NNN level spacing distribution was obtained by us in Ref. [27]. The asymptotic behavior of $P_w^{(2)}(r')$ is different from that of $P_w(r)$: it is $P_w^{(2)}(r') \sim r'^{3\beta+1}$ when r' is small, and $P_w^{(2)}(r') \sim r'^{-3(\beta+1)}$ when r' is large. The Poisson result is $P_p^{(2)}(r') = \frac{6r'}{(1+r')^4}$. Instead of the lengthy analytical results from Wigner-like surmises detailed in Ref. [27], an approximate but precise and useful relation between the probability distribution functions of the NN ratio and the NNN ratio is found as $P_w^{(2)}(r') \approx P_{w,3\beta+1}(r)$ by equating $r = r'$.

It was known that the NN ratio satisfies the functional equation $P(r) = \frac{1}{r^2} P(\frac{1}{r})$, and so does the NNN ratio after replacing r with r' . This property enables us to restrict the study to the range $[0, 1]$ by considering the variables $\tilde{r} = \min\{r, 1/r\}$ and $\tilde{r}' = \min\{r', 1/r'\}$. Thus, the above surmise yields an analytic expression for the mean values $\langle \tilde{r} \rangle_w = 0.386, 0.536, 0.603, 0.676$ and $\langle \tilde{r}' \rangle_w = 0.500, 0.677, 0.734, 0.791$ for the Poisson, GOE, GUE, and GSE, respectively. From these mean values, one can also find $\langle \tilde{r} \rangle_{\text{GSE}} \approx \langle \tilde{r}' \rangle_{\text{GOE}}$, which is just a special case of the $\beta \rightarrow 3\beta + 1$ rule with $\beta = 1$.

The motivation to introduce r' in Ref. [27] is to deal with the case with nearly double degenerate energy levels. When the unperturbed Hamiltonian has double degenerate levels, a small perturbation will lead to nearly double degenerate levels. Then $\langle \tilde{r} \rangle$ can be very close to zero and rapidly changes as the perturbation is increased. However, $\langle \tilde{r}' \rangle$ may remain unchanged, so it becomes a much better criterion to characterize the quantum chaos in this regime. Note that $\langle \tilde{r} \rangle$ and $\langle \tilde{r}' \rangle$ are not expected to satisfy their values listed in Table I in Ref. [27] when the energy levels are nearly doubly degenerate. Namely, when $\langle \tilde{r} \rangle$ is close to zero, $\langle \tilde{r}' \rangle$ will be close to 0.386, 0.536, 0.603, and 0.676. This suggests that if one splits all energy levels into two sets, one set of energy levels satisfies the Poisson, GOE, GUE, and GSE, respectively. For this reason, which was detailed in Ref. [27], both $\langle \tilde{r} \rangle$ and $\langle \tilde{r}' \rangle$ will be evaluated throughout this paper.

B. The ELS of mixed two or four random matrix ensembles

In one case, the unperturbed Hamiltonian has a double degeneracy dictated by a symmetry, then a small perturbation breaks the symmetry, and then the double degeneracy into two nearly degenerated levels. This case was discussed in Sec. II A. In another case, the unperturbed Hamiltonian does not have any level degeneracy, then a small perturbation just breaks some symmetry of the Hamiltonian, and then it will mix different sets of energy levels, which can be labeled by different conserved quantities in the absence of the perturbation. For an infinitesimal perturbation, there is still an obstacle to collecting statistics for individual sets of energy levels. In this section, we investigate the ELS of mixed two or four uncorrelated and identically distributed (UCID) random matrix ensembles [41].

We begin with mixed two UCID random matrix ensembles with size $N = 2$, of which the joint probability distribution function can be written as

$$p(e_1, e_2, e_3, e_4) = p(e_1, e_2)p(e_3, e_4) \propto e^{-\frac{1}{2}(e_1^2+e_2^2)} |e_1 - e_2|^\beta e^{-\frac{1}{2}(e_3^2+e_4^2)} |e_3 - e_4|^\beta, \quad (1)$$

where the level repulsion only exists between e_1 and e_2 , and between e_3 and e_4 .

The ordering of levels can be summarized in the following three independent cases: (i) level ordering $e_1 \leq e_2 \leq e_3 \leq e_4$, with two NN ratios defined as $(e_3 - e_2)/(e_2 - e_1)$ and $(e_4 - e_3)/(e_3 - e_2)$; (ii) level ordering $e_1 \leq e_3 \leq e_2 \leq e_4$, with two NN ratios defined as $(e_2 - e_3)/(e_3 - e_1)$ and $(e_4 - e_2)/(e_2 - e_3)$; and (iii) level ordering $e_1 \leq e_3 \leq e_4 \leq e_2$, with two NN ratios defined as $(e_4 - e_3)/(e_3 - e_1)$ and $(e_2 - e_4)/(e_4 - e_3)$. Other orderings can be related to these three by taking full advantage of

the symmetries in $p(e_1, e_2) = p(e_2, e_1)$ and $p(e_3, e_4) = p(e_4, e_3)$.

Now, we generalize the r statistics defined in Ref. [42] to mixed two random matrix ensembles; the probability density function of r can be calculated from

$$P_{\text{mix-2}}(r) \propto \int_{e_1 \leq e_2 \leq e_3 \leq e_4} \prod_{i=1}^4 de_i p(e_1, e_2, e_3, e_4) \times \left[\delta\left(r - \frac{e_3 - e_2}{e_2 - e_1}\right) + \delta\left(r - \frac{e_4 - e_3}{e_3 - e_2}\right) \right] + \int_{e_1 \leq e_3 \leq e_2 \leq e_4} \prod_{i=1}^4 de_i p(e_1, e_2, e_3, e_4) \times \left[\delta\left(r - \frac{e_2 - e_3}{e_3 - e_1}\right) + \delta\left(r - \frac{e_4 - e_2}{e_2 - e_3}\right) \right] + \int_{e_1 \leq e_3 \leq e_4 \leq e_2} \prod_{i=1}^4 de_i p(e_1, e_2, e_3, e_4) \times \left[\delta\left(r - \frac{e_4 - e_3}{e_3 - e_1}\right) + \delta\left(r - \frac{e_2 - e_4}{e_4 - e_3}\right) \right], \quad (2)$$

where only three independent cases are considered and the other cases only contribute an overall factor.

After changing variables, the integral in Eq. (2) can be rewritten in a neat form:

$$P_{\text{mix-2}}(r) \propto \int \prod_{i=1}^4 de_i p_s(e_1, e_2, e_3, e_4) \sum_{j=1}^2 \delta(r - r_j), \quad (3)$$

where the NN ratio $r_j = (e_{j+2} - e_{j+1})/(e_{j+1} - e_j)$, and $p_s(e_1, e_2, e_3, e_4) = [p(e_1, e_2, e_3, e_4) + p(e_1, e_3, e_2, e_4) + p(e_1, e_3, e_4, e_2)]/3$ is fully symmetrized in $\{e_n\}$.

The integrals in Eq. (3) can be evaluated analytically, and the results are

$$P_{\text{mix-2}}(r) = A_\beta(r) + \frac{1}{r^2} A_\beta(1/r), \quad (4)$$

where $A_\beta(r)$ ($\beta = 1, 2, 4$) are $A_1(r) = (1+r)[15+31r+34r^2+16r^3-(3+r-4r^3)\sqrt{3(3+4r+4r^2)}]/[4(1+r+r^2)^2 \times (3+4r+4r^2)^{3/2}]$, $A_2(r) = 3[\sqrt{3} - (21+70r+92r^2+88r^3+40r^4+16r^5)(3+4r+4r^2)^{-5/2}]/[2\pi(1+r+r^2)]$, and $A_4(r) = [11+33r+39r^2+23r^3+39r^4+33r^5+11r^6-3\sqrt{3}(1+2r)(279+1953r+7467r^2+18731r^3+33883r^4+45581r^5+46551r^6+36224r^7+22172r^8+11736r^9+6712r^{10}+4128r^{11}+2144r^{12}+672r^{13}+96r^{14}) \times (3+4r+4r^2)^{-9/2}]/[2\sqrt{3}\pi(1+r+r^2)^4]$.

To investigate the r' statistic of mixed two random matrix ensembles, one needs to consider the size $N = 3$ case, and the joint probability distribution function can be written as

TABLE I. List of numerical values of averages $\langle \tilde{r} \rangle$ and $\langle \tilde{r}' \rangle$ for the mixed two UCID random matrix ensembles. The values of $\langle \tilde{r} \rangle_W$ and $\langle \tilde{r}' \rangle_W$ are calculated from the derived $N = 2$ surmise and the $N = 3$ surmise, respectively. The values of $\langle \tilde{r} \rangle_{\text{num}}$ and $\langle \tilde{r}' \rangle_{\text{num}}$ are calculated from diagonalizing the corresponding mixed two GOE (real), GUE (complex), and GSE (quaternion) matrix ensembles of size $N = 1000$ with Gaussian distributed entries, averaged over 10^5 histograms. It is interesting to see that they are slightly above the corresponding Poisson values: $\langle \tilde{r} \rangle_P \approx 0.386$ and $\langle \tilde{r}' \rangle_P \approx 0.5$.

Mix-2	$\beta = 1$	$\beta = 2$	$\beta = 4$
$\langle \tilde{r} \rangle_W$	0.423	0.421	0.394
$\langle \tilde{r}' \rangle_W$	0.600	0.649	0.709
$\langle \tilde{r} \rangle_{\text{num}}$	0.424	0.422	0.410
$\langle \tilde{r}' \rangle_{\text{num}}$	0.599	0.650	0.706

$$\begin{aligned}
 p(e_1, e_2, e_3, e_4, e_5, e_6) &= p(e_1, e_2, e_3)p(e_4, e_5, e_6) \\
 &\propto e^{-\frac{1}{2}(e_1^2+e_2^2+e_3^2)}|(e_1 - e_2)(e_1 - e_3)(e_2 - e_3)|^\beta \\
 &\quad \times e^{-\frac{1}{2}(e_4^2+e_5^2+e_6^2)}|(e_4 - e_5)(e_4 - e_6)(e_5 - e_6)|^\beta. \quad (5)
 \end{aligned}$$

After considering all the possible energy level orderings, the probability density function $P_{\text{mix-2}}(r')$ can be expressed as

$$P_{\text{mix-2}}(r') \propto \int \prod_{i=1}^6 de_i p_s(e_1, \dots, e_6) \sum_{j=1}^2 \delta(r - r'_j), \quad (6)$$

where the NNN ratio $r'_j = (e_{j+4} - e_{j+2})/(e_{j+2} - e_j)$, and $p_s(e_1, e_2, e_3, e_4, e_5, e_6) = [p(e_1, e_2, e_3, e_4, e_5, e_6) + p(e_1, e_2, e_4, e_3, e_5, e_6) + p(e_1, e_3, e_4, e_2, e_5, e_6) + \dots]/10$ is fully symmetrized in $\{e_n\}$.

Just like the calculation of $P_{\text{mix-2}}(r)$, $P_{\text{mix-2}}(r')$ can be evaluated exactly. Although the analytical result is lengthy, the numerical evaluation of the integration is rather easy. Similarly to the discussion in Sec. II A, $\tilde{r} = \min\{r, 1/r\}$ and $\tilde{r}' = \min\{r', 1/r'\}$ can be defined in the mixed case also. The mean values of $\langle \tilde{r} \rangle$ and $\langle \tilde{r}' \rangle$ are listed in Table I. These results will be used to distinguish the chaos regime from the integrable regime for the two-colored hybrid SYK models to be discussed in Sec. IV.

In the same manner, the ELS of mixed four UCID random matrix ensembles with $N = 2$ can be studied. We skip the analytical calculations for the probability density

TABLE II. The same as Table I, but using the r statistic for the mixed four UCID random matrix ensemble. They seem quite insensitive to the values of β . They are closer to the corresponding Poisson values than the mixed two matrix case listed in Table I.

Mix-4	$\beta = 1$	$\beta = 2$	$\beta = 4$
$\langle \tilde{r} \rangle_{\text{num}}$	0.396	0.393	0.389
$\langle \tilde{r}' \rangle_{\text{num}}$	0.535	0.537	0.533

TABLE III. The ELS and degeneracy of the two-colored SYK model. The degeneracy $d = 1$ is at a given parity sector (Q_1, Q_2) . The total degeneracy d_t is at a total parity sector $Q_t = Q_1 + Q_2$. (a) N -even case: When $N \pmod{4} = 0$, P maps (Q_1, Q_2) to itself. When $N \pmod{4} = 2$, P maps (Q_1, Q_2) into $(Q_1 + 1, Q_2 + 1)$. (b) N -odd case: When $N \pmod{4} = 1$, P_z maps (Q_1, Q_2) to itself, and P maps (Q_1, Q_2) into $(Q_1 + 1, Q_2 + 1)$. When $N \pmod{4} = 3$, P maps (Q_1, Q_2) to itself, and P_z maps (Q_1, Q_2) into $(Q_1 + 1, Q_2 + 1)$. So P and P_z exchange their roles in the two cases of odd N . Therefore, d_t is the degeneracy in the enlarged Hilbert space, which may not be seen in the exact diagonalization in the minimum Hilbert space, which is defined without adding the two Majorana fermions at ∞ . When doing exact diagonalization in the minimum Hilbert space, only the $d_t = 2$ at $N \pmod{4} = 2$ case can be seen, as shown in Figs. 3(a) and 3(b). However, the $d_t = 1 + 1$ at $N \pmod{4} = 1, 3$ cases cannot be seen (see also Appendix A).

$N \pmod{4}$	0	1	2	3
ELS	GOE	GOE	GUE	GOE
β	1	1	2	1
(Q_1, Q_2)	$d = 1$	$d = 1$	$d = 1$	$d = 1$
$Q_t = Q_1 + Q_2$	$d_t = 1$	$d_t = 1 + 1$	$d_t = 2$	$d_t = 1 + 1$

function, and only list the numerical results of $\langle \tilde{r} \rangle$ and $\langle \tilde{r}' \rangle$ in Table II. In all the cases of $\beta = 1, 2, 4$, we obtain $\langle \tilde{r} \rangle \approx 0.39$ and $\langle \tilde{r}' \rangle \approx 0.535$, which are quite insensitive to the values of β , so the differences between the mixed four GOE/GUE/GSE are almost washed away. They are also different from those in the mixed two UCID random matrix ensembles listed in Table I. When comparing with the Poisson results $\langle \tilde{r} \rangle_P \approx 0.386$ and $\langle \tilde{r}' \rangle_P \approx 0.5$, it is easy to see that even though the $\langle \tilde{r} \rangle$ value is very close to the Poisson result, $\langle \tilde{r}' \rangle$ is still easily distinguishable from the Poisson value (in fact, it is quite close to the GOE value of $\langle \tilde{r} \rangle = 0.5359$). This fact will be used to distinguish the chaos regime from the integrable regime for the four-colored hybrid SYK models to be discussed in Sec. VI.

TABLE IV. The ELS and degeneracy of the four-colored SYK model. The degeneracy $d = 1$ is in a given parity sector $(Q_{12}, Q_{23}, Q_{34}, Q_{0r})$. Q_{0r} is defined only when N is odd. The total degeneracy d_t is in a total parity sector (Q_t, Q_{0r}) . When N is odd, the P_z operator in Eq. (22) maps (Q_{12}, Q_{23}, Q_{34}) to a different parity sector $(Q_{12} + 1, Q_{23} + 1, Q_{34} + 1)$. However, both sets have the same total parity, (Q_t, Q_{0r}) . So, $d_t = 2$. When performing exact diagonalization with a P_{12} and P_{34} basis, both sets $d_t = 2$ can be seen and were shown in Figs. 7(a) and 7(c) (see also Appendix B).

$N \pmod{4}$	0	1	2	3
ELS	BDI	AI	CI	AI
(β, α)	(1,0)	(1,-)	(1,1)	(1,-)
$(Q_{12}, Q_{23}, Q_{34}, Q_{0r})$	$d = 1$	$d = 1$	$d = 1$	$d = 1$
(Q_t, Q_{0r})	$d_t = 1$	$d_t = 2$	$d_t = 1$	$d_t = 2$

III. THE TWO-COLORED $q=4$ SYK

The two-colored $a = 1, 2$ SYK with $q_1 = q_2 = 2$ and $N_1 = N_2 = N$ can be written as

$$H_{1122} = \sum_{i < j; k < l}^N J_{ij;kl} \chi_{1i} \chi_{1j} \chi_{2k} \chi_{2l}, \quad (7)$$

where $J_{ij;kl} = -J_{ji;kl} = -J_{ij;lk}$ are real and satisfy the Gaussian distribution with the mean value $\langle J_{ij;kl} \rangle = 0$ and variance $\langle J_{ij;kl}^2 \rangle = 2J^2/N^3$.

At first sight, no matter if N is even or odd, one can always introduce N complex fermions by combining the two colors $c_i = (\chi_{1i} - i\chi_{2i})/\sqrt{2}$ and $c_i^\dagger = (\chi_{1i} + i\chi_{2i})/\sqrt{2}$. Both c_i and c_i^\dagger can be represented by real matrices, and the particle-hole symmetry operator can be defined as $P_{12} = K \prod_{i=1}^N (c_i^\dagger + c_i)$, where K is a complex conjugate operator. This way of pairing Majorana fermions with different colors to form complex fermions is called the intercolor scheme. As is shown in Appendix A, this construction using P_{12} across the two colors is an alternative representation to discuss the symmetry class of the Hamiltonian. However, we choose a different approach, called the intracolor scheme, in the main text. Both approaches have their own advantages, and they are complementary to each other.

Due to the absence of spectral mirror symmetry, two-colored SYK models will be classified in a threefold way. The threefold way classifies three Wigner-Dyson ensembles: GUE, GOE, and GSE. This classification needs an antiunitary operator T_+ , which commutes with the Hamiltonian as well as all compatible conserved quantities. If such a T_+ exists, then if its squared value $(T_+)^2 = +1$, it means the Hamiltonian is a GOE; if its squared value $(T_+)^2 = -1$, it means the Hamiltonian is a GSE. If such a T_+ does not exist, the Hamiltonian must be a GUE.

A. N -even case

In the N -even case, just following Ref. [27], the intracolor scheme needs to split the site i into even and odd sites [see Fig. 1(a)], and then introduce $N_c = N/2$ complex fermions for each color: $c_{1i} = (\chi_{1,2i} - i\chi_{1,2i-1})/\sqrt{2}$ and $c_{1i}^\dagger = (\chi_{1,2i} + i\chi_{1,2i-1})/\sqrt{2}$. The particle-hole symmetry operator can be defined as $P_1 = K \prod_{i=1}^{N_c} (c_{1i}^\dagger + c_{1i})$ or $R_1 = P_1(-1)^{Q_1} = K \prod_{i=1}^{N_c} (c_{1i}^\dagger - c_{1i})$, but using P_1 is enough for the symmetry classification, and R_1 will not lead to any new result. It is easy to show that $P_1 c_{1i} P_1 = \eta c_{1i}^\dagger$, $P_1 c_{1i}^\dagger P_1 = \eta c_{1i}$, $P_1 \chi_{1i} P_1 = \eta \chi_{1i}$, and $P_1^2 = (-1)^{\lfloor N_c/2 \rfloor}$, where $\eta = (-1)^{\lfloor (N_c-1)/2 \rfloor}$. The number operator of color-1 fermions $Q_1 = \sum_{i=1}^{N_c} c_{1i}^\dagger c_{1i}$ is not a conserved quantity, but its parity $(-1)^{Q_1}$ commutes with H_{1122} . The fact that $P_1 Q_1 P_1^{-1} = N_c - Q_1$ also justifies P_1

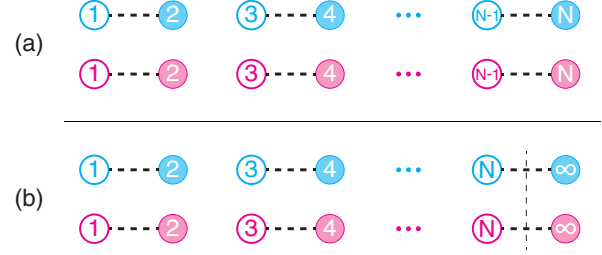


FIG. 1. The two-colored SYK with (a) N even and (b) N odd. Majorana fermions are represented by dots. Each dot has an associated number and color, representing its site index and color index, respectively. A solid dot means the Majorana fermion is represented by a real matrix, while an empty dot means the Majorana fermion is represented by an imaginary matrix. A dashed line connecting them means a complex fermion. In (b), the long vertical dashed line separates the system from two decoupled Majorana fermions added at infinity. The same conventions apply to the other figures.

as an antiunitary particle-hole transformation. One can similarly construct the P_2 operator from color-2 fermions, so it is convenient to characterize the Hilbert space in terms of the conserved joint parities (Q_1, Q_2) , which block-diagonalize it into four sectors: $(Q_1, Q_2) = (\text{Even}, \text{Even})$, $(Q_1, Q_2) = (\text{Even}, \text{Odd})$, $(Q_1, Q_2) = (\text{Odd}, \text{Even})$, and $(Q_1, Q_2) = (\text{Odd}, \text{Odd})$. Unfortunately, neither P_1 nor P_2 commutes or anticommutes with the Hamiltonian, but P_1 , P_2 , R_1 , and R_2 can be used as building blocks to construct operators which will do the job.

To construct an antiunitary operator which commutes or anticommutes with H_{1122} , we introduce

$$P = K \prod_{i=1}^{N_c} (c_{1i}^\dagger + c_{1i})(c_{2i}^\dagger + c_{2i}) = K P_1 P_2, \quad (8)$$

which can be contrasted to the similar operator in the four-colored case [Eq. (18)] to be discussed in Sec. IV. One can show that

$$P \chi_{ai} P = (-1)^{\lfloor \frac{N_c}{2} \rfloor} \eta \chi_{ai} = (-1)^{N_c-1} \chi_{ai}, \quad a = 1, 2. \quad (9)$$

It is easy to see that $P^2 = (-1)^{N_c}$, $P Q_1 P^{-1} = N_c - Q_1$, and $P Q_2 P^{-1} = N_c - Q_2$, and the operator P indeed commutes with the Hamiltonian $[P, H_{1122}] = 0$. Other combinations of P_1 , P_2 , R_1 , and R_2 play exactly the same role as P ; thus, no anticommuting operators exist and spectral mirror symmetry is absent. This is the main difference from the four-colored case to be discussed in Sec. IV, where one can find two antiunitary operators: one P in Eq. (18) commutes, and another P_m in Eq. (20) anticommutes with the Hamiltonian.

For $N \pmod{4} = 0$, $N_c = N/2$ is even, and then P maps the (Q_1, Q_2) sector to the same joint parities sector and $P^2 = 1$, so the ELS is a GOE. The level degeneracy is $d = 1$ in a given (Q_1, Q_2) sector. Because the four sectors

are unrelated, the level degeneracy is $d_t = 1$ in the total parity sector $Q_t = Q_1 + Q_2$.

For $N(\bmod 4) = 2$, $N_c = N/2$ is odd, and then P maps the (Q_1, Q_2) sector to a different joint parities sector with $(Q_1 + 1, Q_2 + 1)$, so the ELS is a GUE. The level degeneracy is $d = 1$ in a given (Q_1, Q_2) sector. However, if we just focus on the total parity Q_t , it is still mapped to the same total parity sector, so it has the $d_t = 2$ double degeneracy [43] in a given total parity sector Q_t . Note that the four sectors can still be separated into two sectors with a given total parity Q_t , which may be useful when we consider a quadratic perturbation such as Eq. (12), which violates the separate parities (Q_1, Q_2) but still conserves the total parity Q_t .

B. N -odd case

When $N(\bmod 4) = 1, 3$, the above procedures for even N need to be modified. In fact, one can still take advantage of the above representation with the N -even case by adding two decoupled Majorana fermions $\chi_{1,N+1} = \chi_{1,\infty}$ and $\chi_{2,N+1} = \chi_{2,\infty}$ to make explicit the parity conservation in color 1 and color 2, respectively [see Fig. 1(b)]. In doing so, one also doubles the Hilbert space when comparing it with the Hilbert space without $\chi_{1,\infty}$ and $\chi_{2,\infty}$. A similar strategy was used before to study the symmetry protected topological phase of a chain of an odd number of Majorana fermions [44] and the ELS of the SYK model with N odd [22]. Then one can still define P_1, P_2 , and P with $N_c = (N + 1)/2$ as before, and Eq. (9) still applies. From the fact that $\chi_{1,\infty}$ and $\chi_{2,\infty}$ do not appear in the Hamiltonian, we have two more building blocks: $Z_1 = P_1 \chi_{1,\infty} = K \prod_{i=1}^{N_c-1} (c_{1i}^\dagger + c_{1i})$ and $Z_2 = P_2 \chi_{2,\infty} = K \prod_{i=1}^{N_c-1} (c_{2i}^\dagger + c_{2i})$, which can be obtained by factoring out $\chi_{1,\infty}$ and $\chi_{2,\infty}$ from P_1 and P_2 , respectively. So when N is odd, P_1, P_2, R_1, R_2 , and Z_1, Z_2 are building blocks to construct various operators.

In addition to the P operator introduced in Eq. (8), another special operator can be constructed for the N -odd case:

$$P_z = K \prod_{i=1}^{N_c-1} (c_{1i}^\dagger + c_{1i})(c_{2i}^\dagger + c_{2i}) = K Z_1 Z_2. \quad (10)$$

One can show that

$$P_z \chi_{ai} P_z = -(-1)^{\lfloor \frac{N_c}{2} \rfloor} \eta \chi_{ai} = (-1)^{N_c} \chi_{ai}, \quad a = 1, 2, \quad (11)$$

where, of course, as usual, $i = \infty$ is always excluded. It is also easy to see that $P_z^2 = (-1)^{N_c-1}$, and P_z still commutes with the Hamiltonian $[P_z, H_{1122}] = 0$. It also leads to $P_z Q_a P_z^{-1} = N_c - 1 - Q_a + 2n_{a\infty}$, where $n_{a\infty} = c_{a\infty}^\dagger c_{a\infty} = 1/2 - i\chi_{a\infty} \chi_{a,N}$ and $a = 1, 2$.

When $N(\bmod 4) = 3$, N_c is even, the P operator maps (Q_1, Q_2) to a sector with the same joint parities, and $P^2 = 1$. So the ELS is a GOE, and the level degeneracy

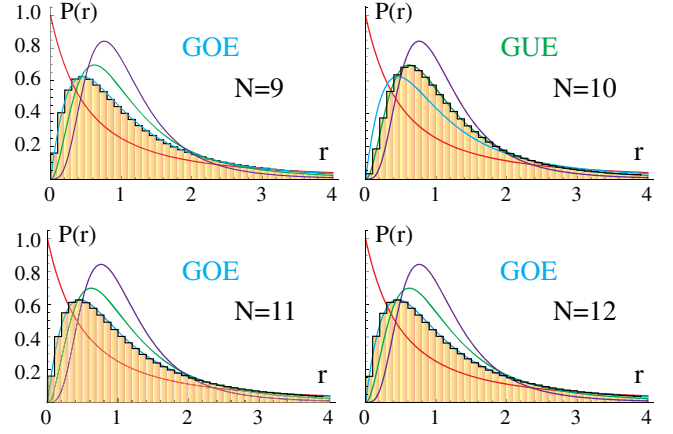


FIG. 2. Distribution of the ratio of consecutive level spacings $P(r)$ for two-colored SYK with various $N = 9, 10, 11, 12$. When $N(\bmod 4) = 1, 2, 3, 0$, the energy level statistics show GOE, GUE, GOE, and GOE, respectively, which agree with the symmetry analysis summarized in Table III. The four background curves are the $P(r)$'s of Poisson (red), GOE (blue), GUE (green), and GSE (purple).

$d = 1$ at a given parities sector (Q_1, Q_2) . When using the P_z operator in Eq. (10), which maps (Q_1, Q_2) to a sector with opposite joint parities $(Q_1 + 1, Q_2 + 1)$, one can conclude that the double degeneracy $d_t = 1 + 1$ in a given total parity sector Q_t .

When $N(\bmod 4) = 1$, N_c is odd, the P_z operator maps (Q_1, Q_2) to a sector with the same joint parities, and $P_z^2 = 1$. So the ELS is still a GOE, and the level degeneracy $d = 1$ at a given parities sector (Q_1, Q_2) . While the P operator maps (Q_1, Q_2) to a sector with opposite parities $(Q_1 + 1, Q_2 + 1)$, one can conclude the double degeneracy $d_t = 1 + 1$ in a given total parity sector Q_t .

In summary, when N is even, there are two cases: when $N(\bmod 4) = 0$, the ELS is a GOE; when $N(\bmod 4) = 2$, the ELS is a GUE. One uses the P operator [Eq. (8)] in both cases. When N is odd, one may need to add a decoupled Majorana fermion at infinity for each color. There are also two cases; both cases are GOEs. When $N(\bmod 4) = 3$, one still uses the P operator [Eq. (8)], but when $N(\bmod 4) = 1$, one must use the P_z operator [Eq. (10)]. These theoretical results are listed in Table III and are confirmed by the exact diagonalizations shown in Fig. 2.

IV. HYBRID TWO-COLORED $q=2$ AND $q=4$ SYK MODEL

In the following, we will discuss a (Q_1, Q_2) parity-violating hybrid two-colored SYK model Eq. (12) which still conserves the total parity Q_t . It can be used to study the stability of quantum chaos and the Kolmogorov-Arnold-Moser theorem in the $f = 2$ -colored SYK models [27]. Furthermore, one can demonstrate the importance of identifying the maximal symmetry, the largest conserved quantities and the minimal Hilbert space to perform the

correct classifications in the RMT. A small-perturbation $K/J \rightarrow 0$ limit which breaks (Q_1, Q_2) but conserves $Q_t = Q_1 + Q_2$ may also be used to drag out the rich and novel physics encoded in Table III from a very effective angle. This kind of small perturbation may also be used to probe the interior of a dual black hole in the bulk [45].

A two-colored $q = 2$ and $q = 4$ hybrid SYK model is hybrid from H_{1122} and H_{12} :

$$H_{1122}^{Hb} = \sum_{i < j; k < l}^N J_{ij;kl} \chi_{1i} \chi_{1j} \chi_{2k} \chi_{2l} + i \sum_{i,j}^N K_{i,j} \chi_{1i} \chi_{2j}, \quad (12)$$

where $J_{ij;kl}$, $K_{i,j}$ are real and satisfy the Gaussian distribution with $\langle J_{ij;kl} \rangle = 0$, $\langle J_{ij;kl}^2 \rangle = 4J^2/N^3$ and $\langle K_{i,j} \rangle = 0$, $\langle K_{i,j}^2 \rangle = 2K^2/N$, respectively. Of course, other hybrid two-colored models can be constructed, but Eq. (12) is the most democratic one between the two colors. For the hybrid model, parities (Q_1, Q_2) do not conserve separately anymore, but the total parity Q_t remains conserved. However, P in Eq. (8) [or Z in Eq. (10) for $N \pmod{4} = 1$] does not commute with H_{1122}^{Hb} anymore due to $\{P, H_{12}\} = 0$ (or $\{Z, H_{12}\} = 0$); thus, different operators are needed to classify Eq. (12).

A. N -even case

When N is even, $N_c = N/2$, we can still take advantage of the building blocks in Sec. III and construct the following operator:

$$P_m = K \prod_{i=1}^{N_c} (c_{1i}^\dagger + c_{1i})(c_{2i}^\dagger - c_{2i}) = KP_1 R_2. \quad (13)$$

Then one can show that

$$\begin{aligned} P_m \chi_{1i} P_m &= (-1)^{\lfloor \frac{N_c}{2} \rfloor + N_c} \eta \chi_{1i} = -\chi_{1i}, \\ P_m \chi_{2i} P_m &= -(-1)^{\lfloor \frac{N_c}{2} \rfloor + N_c} \eta \chi_{2i} = \chi_{2i}. \end{aligned} \quad (14)$$

Due to the opposite signs in the two colors, one can show that $[P_m, H_{12}] = 0$. It is obvious that $[P_m, H_{1122}] = 0$; thus one can conclude that P_m commutes with the hybrid Hamiltonian $[P_m, H_{1122}^{Hb}] = 0$. Since $P_m Q_1 P_m^{-1} = N_c - Q_1$ and $P_m Q_2 P_m^{-1} = N_c - Q_2$, one can show that $P_m Q_t P_m^{-1} = 2N_c - Q_t$ and P_m always map to the same total parity sector and $P_m^2 = 1$ always holds. So, surprisingly or counter-intuitively, in sharp contrast to all the type-I hybrid SYK models studied in Ref. [27], the hybrid system is a GOE at a given total parity sector. This is exactly what is observed in Fig. 3.

For $N \pmod{4} = 2$ in Fig. 3(b), it is instructive to look at the $K/J \rightarrow 0$ limit; H_{1122} at $K/J = 0$ has twofold degeneracy $d_t = 2$, confining it to the total parity Q_t (see Table III). It consists of two sectors (Q_1, Q_2) and

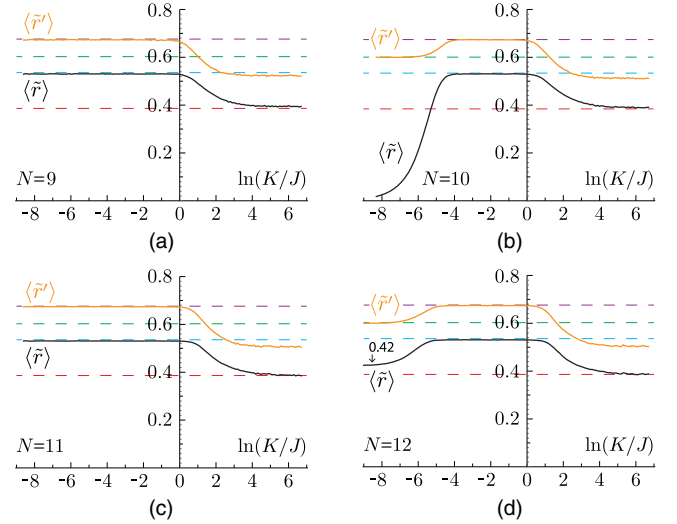


FIG. 3. The averaged value of the \tilde{r} parameter and \tilde{r}' parameter for the hybrid two-colored SYK models with $N = 9, 10, 11, 12$. All the data are taken at a given total parity sector $Q_t = Q_1 + Q_2$ and averaged over 1000, 800, 600, and 400 samples, respectively. The four dashed horizontal lines represent the values 0.386, 0.536, 0.603, 0.676, and, if there is no mixing or nearly double degeneracy, the $\langle \tilde{r} \rangle$'s at those values mean that the ELS is Poisson, GOE, GUE, and GSE, respectively. (a) For $N \pmod{4} = 1$, the graph shows that H_{1122} (namely, at $K/J=0$) is in a GOE. There is a chaotic-to-nonchaotic transition from the GOE to the Poisson as K/J increases. (b) For $N \pmod{4} = 2$, $\langle \tilde{r} \rangle$ (black curve) for NN ELS is rapidly changing, but $\langle \tilde{r}' \rangle$ (orange curve) for NNN ELS shows a nice GUE plateau near $K = 0$. (c) For $N \pmod{4} = 3$, the graph shows similar behaviors to (a). (d) For $N \pmod{4} = 0$, the (slightly above) Poisson-like near $K/J = 0$ will be split into two independent GOEs when projected into two separate parities (Q_1, Q_2) . However, as shown in Sec. II B, the NN ELS and NNN ELS of the mixed ensemble of the two uncorrelated GOE sectors lead to $\langle \tilde{r} \rangle \approx 0.42$ and $\langle \tilde{r}' \rangle \approx 0.6$, listed in Table I. This is indeed observed here. All the chaotic-to-nonchaotic transition is through the GOE due to the P_m symmetry at finite K/J .

$(Q_1 + 1, Q_2 + 1)$, which are mapped to each other by the operator P in Eq. (8). However, as shown in Fig. 2, when we perform the ELS on separate parities (Q_1, Q_2) , then the ELS shows a GUE. Indeed, if we take just one set of energy levels at any ratio of K/J , then the $\langle \tilde{r}' \rangle$ value tells us that the set stays at the GUE until $K/J \sim e^{-6}$. The other set shows identical behavior. As pointed out in Sec. II, when the NN ratio $\langle \tilde{r} \rangle$ is in its GOE value, the corresponding NNN ratio $\langle \tilde{r}' \rangle$ would be close to $\langle \tilde{r} \rangle$'s GSE value; when $\langle \tilde{r} \rangle$ is in Poisson, the $\langle \tilde{r}' \rangle$ would be close to $1/2$. Figure 3(b) shows that the hybrid two-colored SYK is a GOE in some range near $K/J = 1$. And there is a chaotic-to-nonchaotic transition from the GOE to the Poisson as K/J increases.

For $N \pmod{4} = 0$ in Fig. 3(d), in the $K/J \rightarrow 0$ limit, H_{1122} has no degeneracy $d_t = 1$ (see Table III). When performing the exact diagonalization in the total parity sector $(-1)^{Q_t}$, the energy levels in two opposite parity

sectors (Q_1, Q_2) and $(Q_1 + 1, Q_2 + 1)$ are independent of each other and mixed together. Because there is no level repulsion between the energy levels in the two separate parity sectors, the ELS may start to show something close to the Poisson [41]. In Sec. II B, we show that a mixed two GOE indeed leads to $\langle \tilde{r} \rangle \approx 0.423$ and $\langle \tilde{r}' \rangle \approx 0.600$, which agrees with Fig. 3(d) precisely. So, $\langle \tilde{r} \rangle$ and $\langle \tilde{r}' \rangle$ in Fig. 3(d) at small K/J indicate that two uncorrelated GOEs are mixed together. Then, as shown in Fig. 2(b), if one performs the ELS on separate parities (Q_1, Q_2) , then the ELS shows its real face: a GOE. In a given total parity sector, the hybrid two-colored SYK is a GOE in some range near $K/J = e^2$; there is a chaotic-to-nonchaotic transition from the GOE to the Poisson as K/J increases.

B. N -odd case

When N is odd, as in the $q = 4$ case discussed in Sec. III B, after adding $\chi_{1,N+1} = \chi_{1\infty}$ and $\chi_{2,N+1} = \chi_{2\infty}$, one can still define $N_c = (N + 1)/2$. Then Eqs. (13) and (14) still follow, and the discussions following them still hold [46]. So, the hybrid system should be a GOE. In reality, there is a chaotic-to-nonchaotic transition from the GOE to the Poisson as K/J increases.

In order to count the level degeneracy, one may try the following operator by replacing P_1 in Eq. (13) with Z_1 :

$$P'_m = K \prod_{i=1}^{N_c-1} (c_{1i}^\dagger + c_{1i}) \prod_{i=1}^{N_c} (c_{2i}^\dagger - c_{2i}) = KZ_1R_2. \quad (15)$$

Then one can show that

$$\begin{aligned} P'_m \chi_{1i} P'_m &= P_m \chi_{1i} P_m = -\chi_{1i}, \\ P'_m \chi_{2i} P'_m &= P_m \chi_{2i} P_m = \chi_{2i}, \end{aligned} \quad (16)$$

where, as usual, $i = \infty$ is always excluded. Then one can show that $[P'_m, H_{12}] = 0$ and $[P'_m, H_{1122}] = 0$. One can also show that $P'_m Q_1 P'^{-1}_m = (N_c - 1) - Q_1 + 2n_{1\infty}$ and $P'_m Q_2 P'^{-1}_m = N_c - Q_2$, so $P'_m Q_i P'^{-1}_m = (2N_c - 1) - Q_i + 2n_{1\infty}$ always maps to the opposite total parity sector, and it can only be used to establish the energy spectrum between opposite total parity sectors in the hybrid model [Eq. (12)].

Here, we summarize several salient features in Fig. 3. Just from a symmetry point of view, the hybrid model is always the GOE at a given total parity sector, while the three GOEs in Table III are at a given parity sector (Q_1, Q_2) which is conserved only at the $q = 4$ SYK limit $K/J = 0$. As explained in Table III, $d_t = 1 + 1$ with odd N is in the enlarged Hilbert space, so the degeneracy cannot be seen when one is performing exact diagonalization in minimal Hilbert space, because this basis is the minimal original Hilbert space without introducing $\chi_{1\infty}$ and $\chi_{2\infty}$ (see Appendix A). When $N \pmod{4} = 1, 3$, the GOE at $K/J = 0$ is directly connected to the hybrid GOE; this is why the

GOEs in Figs. 3(a) and 3(c) are the two most robust ones against the H_{12} term among all the figures in Fig. 3.

In a sharp contrast, the GOE at $N \pmod{4} = 0$ cannot be seen even at the $K/J \rightarrow 0$ limit. The energy levels with opposite parity are mixed, so both parity sectors combine to behave like something slightly higher than the Poisson. If one had performed the exact diagonalization just in the total parity sector, it may have led to the conclusion that the $q = 4$ two-colored SYK satisfies the Poisson, hinting it might be integrable. In reality, the quantum chaos is hiding inside the total parity and needs to be dragged out by splitting it into the two separate parity sectors. When comparing the knowledge in Sec. II B, one can find that both $\langle \tilde{r} \rangle$ and $\langle \tilde{r}' \rangle$ indeed match their prediction from a mixed two GOE. The “fake” Poisson will evolve to the GOE, and then there is a chaotic-to-nonchaotic transition from the GOE to the real Poisson. As shown in Fig. 3(c), the “fake” Poisson shows a nice plateau regime near $q = 4$, whose length may be used to quantitatively characterize the stability of the quantum chaos near the $q = 4$ side.

Meanwhile, the double degeneracy $d_t = 2$ in the total parity sector at $N \pmod{4} = 2$ is in the minimal original Hilbert space; this can be seen in the exact diagonalization. Any small K breaks this degeneracy. So, the combination of $\langle \tilde{r} \rangle$ and the new universal ratio $\langle \tilde{r}' \rangle$ first introduced in Ref. [27] is needed to describe the evolution of the ELS. Especially, $\langle \tilde{r}' \rangle$ is needed to quantitatively characterize the stability of the quantum chaos near the $q = 4$ side.

V. THE FOUR-COLORED $q = 4$ SYK

Here, we take four colors $a = 1, 2, 3, 4$ with $q_1 = q_2 = q_3 = q_4 = 1$, $N_1 = N_2 = N_3 = N_4 = N$, and the four-colored $q = 4$ SYK can be written as

$$H_{1234} = \sum_{i,j,k,l}^N J_{i,j,k,l} \chi_{1i} \chi_{2j} \chi_{3k} \chi_{4l}, \quad (17)$$

where $J_{i,j,k,l}$ are real and satisfy the Gaussian distribution with mean value $\langle J_{i,j,k,l} \rangle = 0$ and variance $\langle J_{i,j,k,l}^2 \rangle = 4J^2/N^3$.

In contrast to the two-colored cases, the separate parity in each color Q_a , $a = 1, 2, 3, 4$, is not conserved anymore, but the parities of any sum of two (there are six of these) are conserved. Only three out of the six are independent. Without losing any generality, we can just pick the following three as a set: (Q_{12}, Q_{23}, Q_{34}) . Just like with the two-colored SYK model discussed in Sec. III, an intercolor scheme description introduces N complex fermions from the first two colors, 1 and 2, and another N complex fermions from the other two colors, 3 and 4. As is shown in Appendix B, this construction using P_{12} and P_{34} across two of the four colors is an alternative representation for discussing the symmetry class of the Hamiltonian. In the following section, we mainly focus on the intracolor

scheme, which keeps the conserved parity (Q_{12}, Q_{23}, Q_{34}) explicitly, so there are eight sectors which can still be regrouped into two sectors with two different total parities, $Q_t = Q_{12} + Q_{34}$. Both approaches have their own advantages, and they are complementary to each other.

Due to a possible spectral mirror symmetry, the four-colored SYK models will be classified in a tenfold way. The tenfold-way classification can be viewed as a generalization of Wigner-Dyson's threefold way, and it is also known as Altland-Zirnbauer classification theory [47,48]. Thanks to the one-to-one correspondence between each ensemble and symmetric spaces in Cartan's classification, we can label the ten RMT classes by their Cartan names. The classification needs to consider two antiunitary operators T_+, T_- and one unitary operator Λ . T_+ commutes with the Hamiltonian as well as all compatible conserved quantities, while T_- and Λ anticommute with the Hamiltonian but commute with all compatible conserved quantities. Notice that if both T_+ and T_- exist, then $\Lambda = T_+T_-$ always exists as well, but the converse is not true. Ten RMT classes can be identified by the following operator algebra:

- (i) T_- and Λ do not exist: If T_+ exists and $T_+^2 = +1$, the Hamiltonian belongs to class AI (GOE). If T_+ exists and $T_+^2 = -1$, the Hamiltonian belongs to class AII (GSE). If T_+ also does not exist, the Hamiltonian belongs to class AIII (GUE). In fact, this set of classes is reduced to Wigner-Dyson's threefold way discussed in Sec. III.
- (ii) T_+ and T_- exist and $T_+^2 = T_-^2$, or only Λ exists: If $T_+^2 = T_-^2 = +1$, the Hamiltonian belongs to class BDI (chGOE). If $T_+^2 = T_-^2 = -1$, the Hamiltonian belongs to class CII (chGSE). If only Λ exists, the Hamiltonian belongs to class AIII (chGUE). As is written in the parentheses, these are the three chiral ensembles.
- (iii) If T_+ and T_- exist and $T_+^2 \neq T_-^2$, or only T_- exists: If $T_+^2 = -T_-^2 = +1$, the Hamiltonian belongs to class CI (BdG). If $T_+^2 = -T_-^2 = -1$, the Hamiltonian belongs to class DIII (BdG). If T_+ does not exist but T_- exists, with $T_-^2 = +1$, the Hamiltonian belongs to class D (BdG). If T_+ does not exist but T_- exists, with $T_-^2 = -1$, the Hamiltonian belongs to class C (BdG). As is written in the parentheses, these are the four Bogoliubov–de Gennes ensembles.

A. N -even case

In the N -even case, just following the two-colored SYK discussed above, one can split the site i into even and odd sites [Fig. 4(a)], and then introduce $N_c = N/2$ complex fermions for each color: $c_{1i} = (\chi_{1,2i} - i\chi_{1,2i-1})/\sqrt{2}$ and $c_{1i}^\dagger = (\chi_{1,2i} + i\chi_{1,2i-1})/\sqrt{2}$. The particle-hole symmetry operator can be defined as $P_1 = K \prod_{i=1}^{N_c} (c_{1i}^\dagger + c_{1i})$ or $R_1 = K \prod_{i=1}^{N_c} (c_{1i}^\dagger - c_{1i})$. It is easy to show that $P_1^2 = (-1)^{\lfloor N_c/2 \rfloor}$.

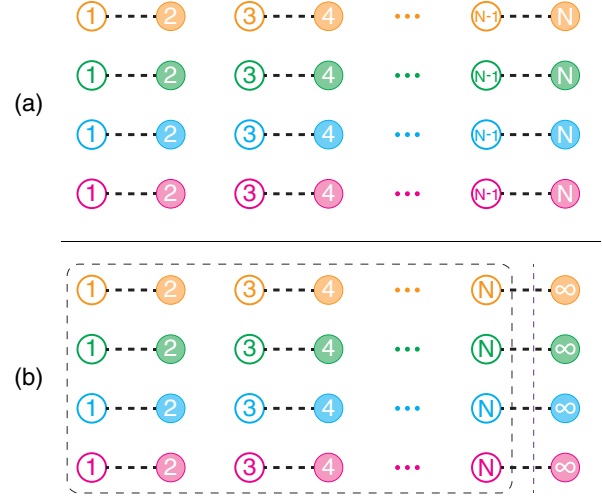


FIG. 4. The four-colored SYK with (a) N even and (b) N odd. In (b), the long vertical dashed line separates the system from the four Majorana fermions added at infinity. The dashed box encloses the additional conserved quantity Q_{0r} . The Hilbert space is enlarged $2^2 = 4$ times. Simultaneously, there are also two more conserved parities.

One can also show that $P_1 c_{1i} P_1 = \eta c_{1i}^\dagger$, $P_1 c_{1i}^\dagger P_1 = \eta c_{1i}$, and $P_1 \chi_{1i} P_1 = \eta \chi_{1i}$, where $\eta = (-1)^{\lfloor (N_c-1)/2 \rfloor}$. Neither the number operator of color-1 fermions $Q_1 = \sum_{i=1}^{N_c} c_{1i}^\dagger c_{1i}$ nor its parity $(-1)^{Q_1}$ is conserved. Very similarly, one can construct P_2, P_3, P_4 and R_2, R_3, R_4 . So P_a, R_a , and $a = 1, 2, 3, 4$, can be used as the building blocks to construct all the possible operators.

Similarly to the antiunitary operator [Eq. (8)] introduced in the two-colored case, we define

$$P = K \prod_{i=1}^{N_c} (c_{1i}^\dagger + c_{1i})(c_{2i}^\dagger + c_{2i})(c_{3i}^\dagger + c_{3i})(c_{4i}^\dagger + c_{4i}) = KP_1 P_2 P_3 P_4. \quad (18)$$

It is easy to show that

$$P \chi_{ai} P = (-1)^{\lfloor \frac{N_c}{2} \rfloor + N_c} \eta \chi_{ai} = -\chi_{ai}, \quad a = 1, 2, 3, 4, \quad (19)$$

which leads to $[P, H_{1234}] = 0$. It is also easy to check that $P^2 = 1$ and $P Q_a P^{-1} = N_c - Q_a$, $a = 1, 2, 3, 4$, which automatically leads to $P Q_{12} P^{-1} = 2N_c - Q_{12}$, $P Q_{23} P^{-1} = 2N_c - Q_{23}$, and $P Q_{34} P^{-1} = 2N_c - Q_{34}$. Obviously, operator P always maps (Q_{12}, Q_{23}, Q_{34}) to the same parity sector.

In fact, we can identify another antiunitary operator:

$$P_m = K \prod_{i=1}^{N_c} (c_{1i}^\dagger + c_{1i})(c_{2i}^\dagger + c_{2i})(c_{3i}^\dagger + c_{3i})(c_{4i}^\dagger - c_{4i}) = KP_1 P_2 P_3 R_4, \quad (20)$$

which simply replaces P_4 in Eq. (18) with the R_4 operator. It can be contrasted with the similar operator in the two-colored case [Eq. (13)]. It is easy to show that

$$\begin{aligned} P_m \chi_{ai} P_m &= (-1)^{\lfloor \frac{N_c}{2} \rfloor} \eta \chi_{ai} = (-1)^{N_c-1} \chi_{ai}, \quad a = 1, 2, 3, \\ P_m \chi_{4i} P_m &= -(-1)^{\lfloor \frac{N_c}{2} \rfloor} \eta \chi_{4i} = (-1)^{N_c} \chi_{4i}, \end{aligned} \quad (21)$$

which indicates that χ_{4i} has an opposite sign from the other three colors, and this opposite sign leads to $\{P_m, H_{1234}\} = 0$. It is also easy to check that $P_m^2 = (-1)^{N_c}$ and $P_m Q_a P_m^{-1} = N_c - Q_a$, $a = 1, 2, 3, 4$, which automatically leads to $P_m Q_{12} P_m^{-1} = 2N_c - Q_{12}$, $P_m Q_{23} P_m^{-1} = 2N_c - Q_{23}$, $P_m Q_{34} P_m^{-1} = 2N_c - Q_{34}$. Obviously, P_m also maps (Q_{12}, Q_{23}, Q_{34}) to the same parity sector.

Now we find two antiunitary operators—one commuting, and another anticommuting with H_{1234} . From the two antiunitary operators, one can define the chirality operator $\Lambda = P P_m = P_4 R_4 = (-1)^{Q_4}$, which is a unitary operator anticommuting with the Hamiltonian $\{\Lambda, H_{1234}\} = 0$. Of course, any $(-1)^{Q_a}$, $a = 1, 2, 3, 4$ works equally well as the unitary chirality operator. This is clearly intuitive, because H_{1234} in Eq. (17) contains one color each, so it anticommutes with $(-1)^{Q_a}$, $a = 1, 2, 3, 4$.

Overall, when combining P with $P^2 = 1$ and P_m with $P_m^2 = (-1)^{N_c}$, one can see that when $N \pmod{4} = 0, 2$, $N_c = N/2$ is even or odd, so H_{1234} belongs to class BDI or class CI, respectively. These cases have the RMT indices $\beta = 1, \alpha = 0$ and $\beta = 1, \alpha = 1$, respectively. Both show the GOE bulk statistics, but with different edge exponents with $\alpha = 0$ and $\alpha = 1$, respectively. The fact that $P^2 = 1$ also leads to no level degeneracy in the parity sector (Q_{12}, Q_{23}, Q_{34}) . Since there is no operator that can make connections between different parity sectors, the level degeneracy is $d_t = 1$ in the total parity sector Q_t .

B. N -odd case

1. Incomplete classification with a missing conserved quantity

When $N \pmod{4} = 1, 3$, the above procedures for even N need to be modified. In fact, one can still take advantage of the above representation with the N -even case by adding decoupled Majorana fermions $\chi_{a,N+1} = \chi_{a,\infty}$, $a = 1, 2, 3, 4$, to make the parity conservations in (Q_{12}, Q_{23}, Q_{34}) explicitly [see Fig. 4(b)]. Then one can still define P_a , $a = 1, 2, 3, 4$ and R_a , $a = 1, 2, 3, 4$, P , and P_m [and therefore also the chirality operator $\Lambda_a = (-1)^{Q_a}$] with $N_c = (N + 1)/2$ as before. When $N \pmod{4} = 3$, N_c is even, and $P^2 = 1$, $P_m^2 = 1$, it is in class BDI; when $N \pmod{4} = 1$, N_c is odd, and $P^2 = 1$, $P_m^2 = -1$, it is in class CI. Unfortunately, this conclusion is *incorrect*. It could be expected that the Hilbert space is enlarged 4 times. Simultaneously, there should also two more conserved parities when comparing with the total number of conserved quantities in intercolor scheme, which

is 2. We only have three as (Q_{12}, Q_{23}, Q_{34}) , so one conserved quantity is still missing, and we will find this missing parity in Sec. VB 2.

When N is odd, one may also use the following operator:

$$P_z = K Z_1 P_2 Z_3 P_4, \quad (22)$$

which simply replaces P_1, P_3 in Eq. (18) with the Z_1, Z_2 operator. So it will play a complementary role to P , which will be analyzed in the following. One can show that

$$P_z \chi_{ai} P_z = -(-1)^{\lfloor \frac{N_c}{2} \rfloor + N_c} \eta \chi_{ai} = \chi_{ai}, \quad a = 1, 2, 3, 4, \quad (23)$$

where, as usual, $i = \infty$ is always excluded. It is also easy to check that $[P_z, H_{1234}] = 0$, $P_z^2 = -1$, that $P_z Q_a P_z^{-1} = N_c - 1 - Q_a + 2n_{a\infty}$, $a = 1, 3$, and that $P_z Q_a P_z^{-1} = N_c - Q_a$, $a = 2, 4$, which automatically leads to $P_z Q_{12} P_z^{-1} = 2N_c - 1 - Q_{12} + 2n_{1\infty}$, $P_z Q_{23} P_z^{-1} = 2N_c - 1 - Q_{23} + 2n_{3\infty}$, and $P_z Q_{34} P_z^{-1} = 2N_c - 1 - Q_{34} + 2n_{3\infty}$. Obviously, operator P_z maps (Q_{12}, Q_{23}, Q_{34}) to a different parity sector $(Q_{12} + 1, Q_{23} + 1, Q_{34} + 1)$. However, both sets have the same total parity, $Q_t = Q_{12} + Q_{34}$.

2. Complete classification by finding the missing conserved quantity Q_{0t}

Unfortunately, the above classification disagrees with our exact diagonalization results, especially on edge exponents. It is important to resolve the discrepancy. It turns out that it missed the additional conserved quantity Q_{0t} , which is the parity in the square box in Fig. 4(b). In the two-colored cases discussed in Secs. III and IV, it is also a conserved quantity, but it does not commute with parity Q_1 and parity Q_2 , so it cannot be used in the complete set of the conserved quantities. Here, it commutes with the parities Q_{12}, Q_{23}, Q_{34} . So Q_{0t} is the (so far missing) additional member of the complete set of the conserved quantities $(Q_{12}, Q_{23}, Q_{34}, Q_{0t})$. From Fig. 4(b), it is easy to see that

$$Q_t = Q_{12} + Q_{34} = Q_{0t} + n_{12\infty} + n_{34\infty}, \quad (24)$$

where $n_{12\infty}, n_{34\infty}$ may not be able to be conveniently expressed in terms of complex fermions c_i , $i = 1, 2, 3, 4$, but it can always be concisely expressed in terms of Majorana fermions $n_{12\infty} = \frac{1}{2} - i\chi_{1\infty}\chi_{2\infty}$, $n_{34\infty} = \frac{1}{2} - i\chi_{3\infty}\chi_{4\infty}$. Then one can show that

$$\begin{aligned} P Q_{0t} P^{-1} &= 4N_c + 2 - Q_{0t} - 2(n_{12\infty} + n_{34\infty}), \\ P_m Q_{0t} P_m^{-1} &= 4N_c + 1 - Q_{0t} - 2n_{12\infty}. \end{aligned} \quad (25)$$

So, one can see that the P_m operator *changes* the parity of Q_{0t} . This fact eliminates P_m as the valid operator and leaves P as the only valid one, so there is no spectral mirror symmetry in the given parities sector $(Q_{12}, Q_{23}, Q_{34}, Q_{0t})$. Because of $P^2 = 1$ and the lack of spectral mirror

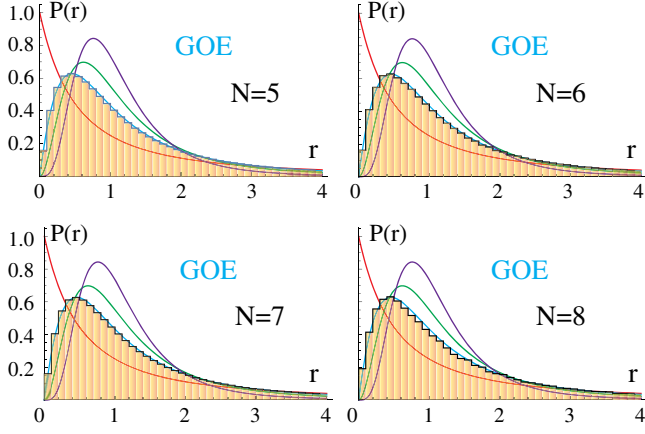


FIG. 5. Distribution of the ratio of consecutive level spacings $P(r)$ for the four-colored SYK model with various $N = 5, 6, 7, 8$. When $N \pmod{4} = 1, 2, 3, 0$, all the bulk ELS show GOEs, which agrees with the symmetry analysis summarized in Table IV. However, they can be distinguished by different edge behaviors, as shown in Fig. 6. The four background curves are the $P(r)$'s of the Poisson (red), GOE (blue), GUE (green), and GSE (purple), respectively.

symmetry, the ELS is class AI (GOE), and no edge exponent can be defined for GOE.

One can also show that

$$P_z Q_{0r} P_z^{-1} = 4N_c - Q_{0r} + 2(n_{1\infty} + n_{3\infty} - n_{12\infty} - n_{34\infty}), \quad (26)$$

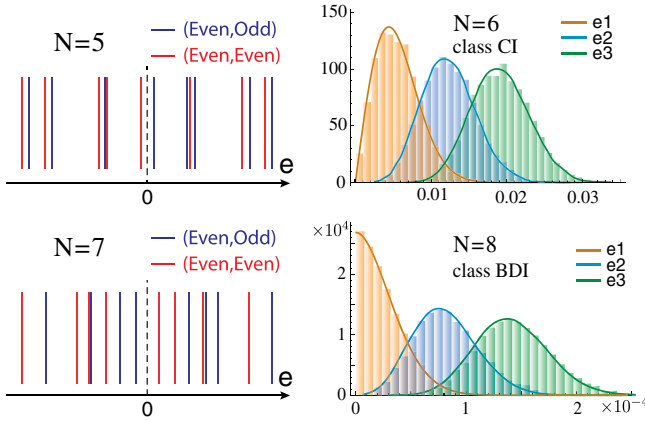


FIG. 6. Distributions of the eigenvalues of the four-colored SYK model with a few of the smallest absolute values. For the $N = 6$ and $N = 8$ cases, each parity sector has mirror symmetry; thus, we calculate the three smallest absolute values and compare them with predictions (solid lines) from RMT classes BDI and CI and find the RMT indices $\alpha = 0, 1$, respectively. For the $N = 5$ and $N = 7$ cases, each parity sector has no mirror symmetry; thus, we have no well-defined α index. To show the absence of the mirror symmetry in the odd- N cases, we plot a few of the smallest absolute eigenvalues in the $(Q_{12}, Q_{34}) = (+, +)$ or $(+, -)$ sector for a single random realization.

which shows that P_z conserves (Q_t, Q_{0r}) . This fact shows that in a given total parity sector (Q_t, Q_{0r}) , the energy level has twofold degeneracy $d_t = 2$. This result could be useful with a quadratic term like in Eq. (27), which breaks the parities, but still keeps the total parity.

In summary, when $N \pmod{4} = 0$, it is in class BDI; when $N \pmod{4} = 2$, it is in class CI. In addition to the bulk, they also have the edge exponents. When $N \pmod{2} = 1, 3$, it is in class AI (GOE) with $d_t = 2$, and no edge exponent can be defined. These theoretical results are confirmed by the exact diagonalization shown in Fig. 5 for the bulk and in Fig. 6 for the hard-edge behavior.

VI. THE HYBRID FOUR-COLORED $q=2$ AND $q=4$ SYK MODEL

Similarly to the two-colored cases, in the following section, we will discuss the parity $(Q_{12}, Q_{23}, Q_{34}, Q_{0r})$ -violating hybrid four-colored SYK model [Eq. (27)]. It still conserves the total parity, (Q_t, Q_{0r}) . It can be used to study the stability of quantum chaos and the Kolmogorov-Arnold-Moser theorem in the $f = 4$ colored SYK [27]. Furthermore, one can demonstrate the importance of identifying the maximal symmetry, the largest conserved quantities, and the smallest Hilbert space in order to perform the correct classifications in the RMT. A small-perturbation $K/J \rightarrow 0$ limit which breaks (Q_{12}, Q_{23}, Q_{34}) but conserves $Q_t = Q_{12} + Q_{34}$ may also be used to drag out the rich and novel physics encoded in Table IV. This kind of small perturbation may also be used to probe the interior of a dual black hole in the bulk [45].

A hybrid four-colored $q = 2$ and $q = 4$ SYK model is

$$H_{1234}^{Hb} = \sum_{i,j,k,l} J_{i,j,k;l} \chi_{1i} \chi_{2j} \chi_{3k} \chi_{4l} + i \sum_{i,j;a<b} K_{i,j} \chi_{ai} \chi_{bj}. \quad (27)$$

Of course, other hybrid four-colored models can also be constructed, but Eq. (27) is the most democratic one among all four colors. In fact, shown in Fig. 7 is our exact diagonalization in a slightly generalized model $H_{1234}^{Hb} = \sum_{i,j,k,l} J_{ijkl} \chi_{1i} \chi_{2j} \chi_{3k} \chi_{4l} + i \sum_{i,j;a<b} K_{ij}^{ab} \chi_{ai} \chi_{bj}$, where K_{ij}^{ab} also depends on colors but satisfies the same distribution. Our exact diagonalization on Eq. (27) leads to similar results with slightly more noise on a given distribution.

Now, we can apply the particle-hole transformation P and P_m to it. Although the (Q_{12}, Q_{23}, Q_{34}) parities are not conserved anymore, the total parity, $(-1)^{Q_t}$ [and $(-1)^{Q_{0r}}$ when N is odd], remains conserved. It is also easy to see that $\{P_m, H_{12}\} = \{P_m, H_{13}\} = \{P_m, H_{23}\} = 0$ and $[P_m, H_{14}] = [P_m, H_{24}] = [P_m, H_{34}] = 0$. So P_m neither commutes nor anticommutes with H_{1234}^{Hb} . Because $[P, H_{1234}] = [P_z, H_{1234}] = 0$ and $\{P, \sum_{ab} H_{ab}\} = \{P_z, \sum_{ab} H_{ab}\} = 0$, the hybrid four-colored SYK does not have any symmetry anymore. This is in sharp contrast to the hybrid two-colored SYK [Eq. (12)], where one can still

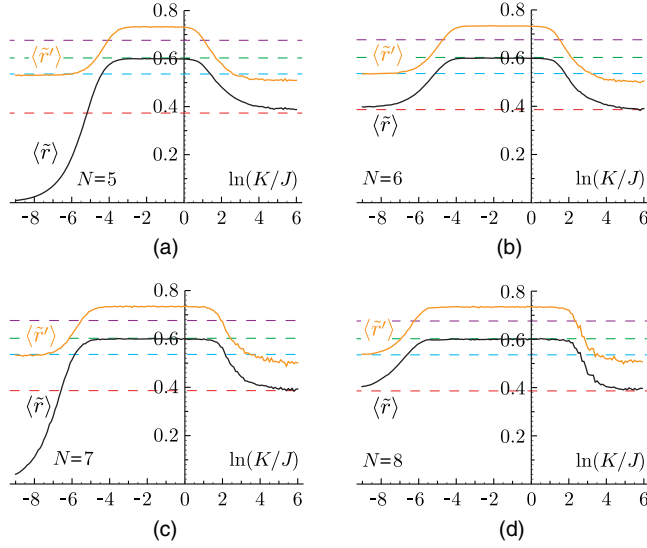


FIG. 7. The mean value of the \tilde{r} and \tilde{r}' parameters for the four-colored hybrid SYK models with $N = 5, 6, 7, 8$. All data are taken at a given total parity sector $Q_t = Q_1 + Q_2$ and averaged over 400, 200, 10, and 6 samples, respectively. For $N \pmod 4 = 1, 3$ in (a) and (c), the H_{1234} (namely, at $K = 0$) has twofold degeneracy $d_t = 2$ in the total parity sector. $\langle \tilde{r} \rangle$ (black curve) for NN ELS is rapidly changing, but $\langle \tilde{r}' \rangle$ (orange curve) for NNN ELS shows a nice GOE plateau near $K = 0$. The hybrid SYK is in the GUE within some range near $K/J = 1$, and there is a chaotic-to-nonchaotic transition from the GUE to the Poisson as K/J increases. As shown in Ref. [27], when $\langle \tilde{r} \rangle$ is at the GUE ($\beta = 2$) value 0.6027, $\langle \tilde{r}' \rangle$ would be close to the value 0.7344. When $\langle \tilde{r} \rangle$ is at the Poisson value 0.3863, $\langle \tilde{r}' \rangle$ would be close to $1/2$, which is slightly below the $\langle \tilde{r} \rangle$'s GOE value of 0.5359. For $N \pmod 4 = 2, 0$ in (b) and (d), as explained in Sec. II B and the text, the section very slightly above the Poisson values on the left near the $q = 4$ side is due to the mixing of four uncorrelated parity sectors. The quantum chaos in the GOE is hidden in this “fake” Poisson and can be dragged out by doing ELS on a given parity sector (Q_{12}, Q_{23}, Q_{34}), while the Poisson on the right near the $q = 2$ side is a true one. As listed in Table II, the NNN ELS of the four mixed uncorrelated sectors lead to $\langle \tilde{r}' \rangle \approx 0.535$, which is quite close to the GOE value of $\langle \tilde{r} \rangle = 0.5359$. Indeed, \tilde{r}' shows a plateau for the GOE at small K/J .

identify a conserved quantity P_m [Eq. (13)]. Just from a symmetry point of view, the hybrid four-colored SYK belongs to the class A (GUE), so the ELS may satisfy GUE for any ratio of K/J . When performing the exact diagonalization, we need to look at a given total parity $(-1)^{Q_t}$. However, the Kolmogorov-Arnold-Moser theorem shows that as K/J increases to $(K/J)_c$, there may be a chaotic-to-nonchaotic transition from the GUE to the Poisson. Our exact diagonalization studies shown in Fig. 7 confirm this picture.

A. N -even case

It is instructive to look at the $K/J \rightarrow 0$ limit in Figs. 7(b) and 7(d). If one just focuses on the total parity sector $(-1)^{Q_t}$,

then as shown in Table IV, there is no level degeneracy and $d_t = 1$. When $N \pmod 4 = 0, 2$, the exact diagonalization is performed in the total parity sector Q_t . There are four separate parities in (Q_{12}, Q_{23}, Q_{34}) falling within the same total parity sector Q_t , and these four sectors are completely independent of each other. Since there is no level repulsion among the four sets of energy levels, the ELS may start to show something similar to (in fact, very slightly above) the Poisson [41]. This is indeed the case shown in Figs. 7(b) and 7(d). Naively, this could mislead one to the conclusion that H_{1234} may be integrable when $N \pmod 4 = 0, 2$. Note that here it is four sectors that are mixed together in the same total parity sector Q_t , while only two sectors are mixed in the two-colored case, so the four-colored case is expected to be more close to the Poisson than the two-colored case. Indeed, in Sec. II B and Table II, we show that the mixed four UCID GOE, GUE, and GSE, all lead to $\langle \tilde{r} \rangle \approx 0.39$ and $\langle \tilde{r}' \rangle \approx 0.535$, which agree with Figs. 7(b) and 7(d). So the values of $\langle \tilde{r} \rangle$ and $\langle \tilde{r}' \rangle$ in Figs. 7(b) and 7(d) at small K/J mean that four uncorrelated GOEs are mixed together. However, as shown in Fig. 5, if one performs the ELS on separate parities (Q_{12}, Q_{23}, Q_{34}), then the ELS shows its real face: class BDI and class CI.

As K/J increases to $(K/J)_c$, there is a crossover from the “fake” Poisson to the GUE, then followed by a chaotic-to-nonchaotic transition from the GUE to the real Poisson near $q = 2$. As shown in Figs. 7(b) and 7(d), the “fake” Poisson shows a nice plateau regime in both values of $\langle \tilde{r} \rangle$ and $\langle \tilde{r}' \rangle$ near $q = 4$, whose length may be used to quantitatively characterize the stability of the quantum chaos near the $q = 4$ side.

B. N -odd case

Similarly, one can first look at the $K/J \rightarrow 0$ limit in Figs. 7(a) and 7(c). As shown in Table IV, when $N \pmod 4 = 1, 3$, due to the existence of the P_z operator, which maps ($Q_{12}, Q_{23}, Q_{34}, Q_{0t}$) to ($Q_{12} + 1, Q_{23} + 1, Q_{34} + 1, Q_{0t}$), there is a double degeneracy $d_t = 2$. The degeneracy is broken by any nonzero K/J . However, as shown in the previous section, when performing the ELS on separate parities ($Q_{12}, Q_{23}, Q_{34}, Q_{0t}$), the ELS shows the GOE [Figs. 5(b) and 5(d)]. The evolution and fine structures characterized by the NN ratio $\langle \tilde{r} \rangle$ and NNN ratio $\langle \tilde{r}' \rangle$ are shown in Figs. 7(a) and 7(c). Especially, $\langle \tilde{r}' \rangle$ is needed to quantitatively characterize the stability of the quantum chaos near the $q = 4$ side. As K/J increases to $(K/J)_c$, there is a crossover from the GOE to the GUE, then followed by a chaotic-to-nonchaotic transition from the GUE to the real Poisson near $q = 2$.

VII. PERSPECTIVES AND DISCUSSIONS

As mentioned in the Introduction, during the last decade, since the discovery of the topological insulators [1,2], there have also been extensive research activities on the classification of topological phases of matter which break no

symmetries [3,4]. These phases also split into two classes: interacting symmetry protected topological (SPT) phases with trivial bulk order (short-range entanglement) and symmetry enriched topological (SET) phases with non-trivial bulk topological order (long-range entanglement) [3,4]. In some special cases, the Hamiltonian whose exact ground states show such SPT or SET orders can be constructed, but these Hamiltonians, in general, involve highly nonlocal interactions which are needed to stabilize such states. In most cases, the Hamiltonians which may host these phases are not known; the classifications are purely symmetry based. For a general, simple experimental accessible Hamiltonian, these states may have much higher energy than conventional symmetry-broken states.

A dual vortex method (DVM) was developed in Refs. [49–52] to classify all the possible Mott insulating phases of interacting bosons hopping in various 2D lattices at generic commensurate filling factors $f = p/q$ (p, q are relative prime numbers). The DVM is a magnetic space group (MSG) symmetry-based approach which, in principle, can be used to classify all the possible phases and phase transitions in an extended boson Hubbard (EBHM) model. But whether a particular phase identified by the DVM will become a stable ground state or not depends on the specific values of all the possible parameters in the EBHM. This kind of question can only be addressed by a microscopic approach such as quantum Monte Carlo simulations on a specific Hamiltonian. The combination of both methods is needed to completely understand quantum phases and phase transitions in the EBHM. A similar approach was extended to 3D (called a vortex condensation approach) to classify SPT phases in $(3 + 1)D$ [3,4,53].

The possible organization patterns of matter can also be classified from a different perspective: they can also be classified by how quantum information is scrambled in the system. So, in this paper, we took a different route and achieved different goals: we classify different types of quantum chaos and quantum information scramblings in the colored SYK models instead of their topologically equivalent classes by using the RMT. Here, we have already written down a realistic colored SYK Hamiltonian and identified its maximal symmetries, the largest number of conserved quantities (which are various fermion parities), and the smallest (irreducible) Hilbert space. In particular, one must also exhaust all the possible antiunitary operators which commute or anticommute with the Hamiltonian. There are also two kinds of such antiunitary operators—the first kind keep all the conserved quantities in the same sector, and the second kind map out of the sector. The former leads to the RMT classification, while the latter establishes the connections between different sectors, and therefore the degeneracy of the energy levels. If any symmetry or conserved quantity or any operator is missed, it can lead to misleading results in both classification and

exact diagonalization results. We achieved such a goal in classifying the quantum chaos in colored SYK with two and with four colors and a balanced number of Majorana fermions among different colors. The color degrees of freedom (d.o.f.) may also be promoted to a global symmetry G , and then the parities are promoted to various conserved quantities, so it is also interesting to see how the color d.o.f. compared to the SYK model with global $G = O(M)$ or $G = U(M)$ symmetries [54]. As shown in Ref. [31], there are some still unknown relations between colored SYK and the colored (Gurau-Witten) tensor model. The method can also be applied in order to perform the RMT classifications of colored tensor models [33].

It is interesting to note that the RMT was originally proposed to study the many-body energy level correlations of a nuclei with a large atomic number to hold a large number of electrons [55,56]. Then it was also used to classify the quantum chaos of noninteracting electrons moving in a random potential which may show a metal-to-Anderson-insulator transition (MIT) [57]. There is a corresponding chaotic-to-nonchaotic transition, where the single-particle ELS satisfies the Wigner-Dyson distribution in the metal, while it satisfies the Poisson in the Anderson insulator. RMT was first applied to QCD in Ref. [58] and was classified in Ref. [59]. In the presence of pairing such as colored superconductivity in QCD, fermion numbers are no longer conserved; only the fermion parities are conserved. So our method may also be applied to perform the RMT descriptions of colored superconductivity in QCD [60,61]. On the other hand, the topologically equivalent classes of the SPT phases of noninteracting electrons such as topological insulators or superconductors can be classified with the same symbols as the tenfold way of the RMT [1,2] in terms of the two possible antiunitary operators. However, for many-body interacting electron systems, the antiunitary operators are not enough; the SPT or SET phases may be classified by using more advanced mathematical tools such as cohomology, cobordism, and tensor categories [3,4], which were already used in rational conformal field theory (RCFT) and also in topological quantum computing.

As shown in this paper, the color d.o.f. make a dramatic difference. This is due to the fact that the color d.o.f. lead to more conserved parities and also more antiunitary or unitary operators. As shown in the text, an even or odd number of Majorana fermions seems to make a lot of difference. Whether the number is even or odd also leads to a different number of mutually conserved parities and different antiunitary or unitary operator contents. In retrospect, the multichannel Kondo models lead to dramatic differences from single-channel Kondo models [62–65], with the channel index playing a similar role to the color index here. Furthermore, only the boundary conditions changing with an odd number of fermions lead to non-Fermi liquid behaviors, and therefore the absence of any

quasiparticles, and we expect that it leads to chaotic behaviors. Meanwhile, the boundary conditions changing with even number of fermions leads to Fermi liquid behaviors with well-defined quasiparticle excitations, and we expect that it leads to nonchaotic behaviors. Of course, an odd number of Majorana fermions leads to nontrivial topology and plays a dramatic role in the classification of topological phases of matter [3,4], while usually an even number of Majorana fermions does not.

As presented in the Introduction, there are at least two different ways to characterize the quantum chaos or quantum information scramblings. One way is to use the Lyapunov exponent (or spectrum) to characterize the quantum information scramblings; they can be extracted by evaluating OTOC functions at an early time, $t_d < t < t_d \log N = t_s$ (namely, between dissipation time and Ehrenfest time), by a large N expansion. It is insensitive to $N \pmod{8}$ Bott periodicity and also the ground-state degeneracy. Another way is to use RMT to characterize energy level statistics or spectral form factors in a tenfold way at a finite and large enough N which shows $N \pmod{8}$ Bott periodicity and also the ground-state degeneracy. The many-body energy level spacing $\Delta E \sim e^{-N}$, so the RMT describes the energy level correlations at the Heisenberg timescale, $t_H \sim 1/\Delta E \sim e^N$. Because of the wide separation of the two timescales t_s and t_H , it remains an open problem to explore the relations between the two schemes. It was believed that the two schemes are complementary to each other to characterize the quantum chaos of a system from different perspectives. So, it remains an outstanding problem to investigate the connections between the results achieved by RMT here with those achieved by the OTOC in Ref. [12].

The colored SYK models may also be experimentally realized in various cold atom [66], cavity QED [35], or solid-state systems [67–69] where there may always be color d.o.f. They naturally stand for different band indices in a material. This could achieve the lofty goal of investigating various exotic properties of quantum black holes in just a conventional lab on Earth.

ACKNOWLEDGMENTS

J. Y. thank C. Xu and S. Shenker for helpful discussions. F. S. and J. Y. acknowledge AFOSR No. FA9550-16-1-0412 for support. This research at K. I. T. P. was supported in part by the National Science Foundation under Grant No. NSF PHY-1748958. Y. Y.-X. and W.-M. L. are supported in part by the National Key R&D Program of China under Grants No. 2016YFA0301500, NSFC under Grants No. 11434015, No. 61227902. Y. Y.-X. is also supported by China Postdoctoral Science Foundation under Grant No. 2018M640190.

Note added.—Recently, two of the authors found that the two-colored SYK models may find an application in traversable wormholes with an attractive interaction [70].

APPENDIX A: TWO-COLORED SYK MODEL: THREEFOLD WAY AND OPERATOR P_{12} ACROSS THE TWO COLORS

In the three appendixes, we will give an alternative intercolor pairing presentation to classify the quantum chaos in the two-colored (Fig. 8) and four-colored cases (Fig. 9), and also the corresponding hybrid colored SYK models. It may be a quite natural approach at first sight. It may also be the most convenient and economic basis for doing exact diagonalization, because by pairing across different colors, one can construct the minimal Hilbert space to perform the exact diagonalization no matter if N is even or odd.

However, if N is even, due to the hidden of the separate parity conservations in (Q_1, Q_2) in the two-colored case and (Q_{12}, Q_{23}, Q_{34}) in the four-colored case, special care is needed to identify the complete set of conserved quantities, select the relevant operators to perform the classification, and derive the degeneracy.

If N is odd, one may do the classification in the minimum Hilbert space with a given Q_{12} in the two-colored case or with a given (Q_{12}, Q_{34}) in the four-colored case. To be compared to the results achieved in the main text with the intracolor representation, by adding Majorana fermions at ∞ , one may also perform the classification in the twice enlarged Hilbert space (Q_{12}, \tilde{Q}_{12}) in the two-colored case and in the 4-times enlarged Hilbert space $(Q_{12}, \tilde{Q}_{12}, Q_{34}, \tilde{Q}_{34})$ in the four-colored case.

Obviously, the intercolor scheme is specialized to the balanced case only and cannot be generalized to the imbalanced case, while the approach used in the main text can be easily generalized to the imbalanced case. It is constructive to compare the two (when N is even) or three (when N is odd) different classification schemes, which not only lead to the same conclusions, but also bring considerable additional insights into the physical picture and may have broad impacts on other problems.

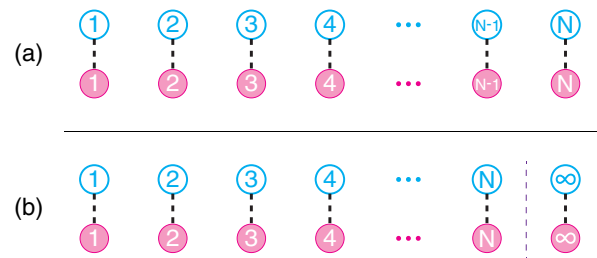


FIG. 8. The two colors with intercolor pairings with (a) N even and (b) N odd, in contrast to the intracolor pairings in the main text. The color-1 fermions are all real, while the color-2 fermions are all imaginary. In (b), the long vertical dashed line separates the system from the two Majorana fermions added at infinity. The Hilbert space in (b) is doubled. Simultaneously, there is also one more conserved parity. Compare with Fig. 1.

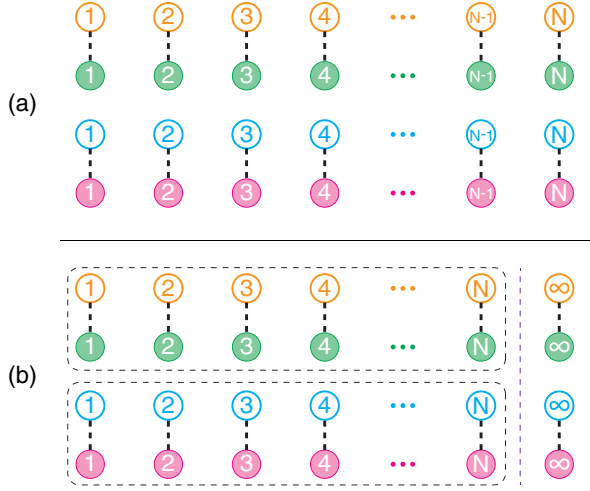


FIG. 9. The four colors with (a) N even and (b) N odd with the intercolor pairings across colors 1 and 2, and across colors 3 and 4. In (b), the long vertical dashed line separates the system from the four Majorana fermions added at infinity. The Hilbert space is enlarged by $2 \times 2 = 4$ times. Simultaneously, there are also two more conserved parities. The two dashed boxes enclose the two conserved parities Q_{12} and Q_{34} .

When N is even, the two schemes are as follows:

- For the two-colored case, the (Q_1, Q_2) intracolor scheme in the main text and the (Q_1, Q_2) intercolor scheme in the appendixes.
- For the four-colored case, the (Q_{12}, Q_{23}, Q_{34}) intracolor scheme in the main text and the (Q_{12}, Q_{23}, Q_{34}) intercolor scheme in the appendixes.

When N is odd, the three schemes are as follows:

- For the two-colored case, the $(\tilde{Q}_1, \tilde{Q}_2)$ intracolor scheme in the main text, the Q_{12} minimum Hilbert intercolor space in the appendixes, and the (Q_{12}, \tilde{Q}_{12}) intercolor scheme in the appendixes.
- For the four-colored case, the $(\tilde{Q}_{12}, \tilde{Q}_{23}, \tilde{Q}_{34}, Q_t)$ intracolor scheme in the main text, the (Q_{12}, Q_{34}) minimum Hilbert intercolor space in the appendixes, and the $(Q_{12}, \tilde{Q}_{12}, Q_{34}, \tilde{Q}_{34})$ intercolor scheme in the appendixes.

At first sight, for both N even and odd, one can always introduce N complex fermions by combining the two colors $c_i = (\chi_{1i} - i\chi_{2i})/\sqrt{2}$ and $c_i^\dagger = (\chi_{1i} + i\chi_{2i})/\sqrt{2}$, and define the particle-hole symmetry operator to be $P_{12} = K \prod_{i=1}^N (c_i^\dagger + c_i) = K \chi_{1,1} \chi_{1,2} \dots \chi_{1,N}$, involving only the color 1. In fact, $R_{12} = P_{12} (-1)^{Q_{12}} = K \prod_{i=1}^N (c_i^\dagger - c_i) = K i \chi_{2,1} i \chi_{2,2} \dots i \chi_{2,N}$, involving only the color 2, works equally well, but it will not lead to new symmetry. It is easy to show that $P_{12}^2 = (-1)^{\lfloor N/2 \rfloor}$. One can also show that $P_{12} c_i P_{12} = \eta c_i^\dagger$, $P_{12} c_i^\dagger P_{12} = \eta c_i$, and $P_{12} \chi_{ai} P_{12} = \eta \chi_{ai}$, $a = 1, 2$, where $\eta = (-1)^{\lfloor (N-1)/2 \rfloor}$. The total number of fermions $Q_t = \sum_{i=1}^N c_i^\dagger c_i$ is not a conserved quantity, but the parity $(-1)^{Q_t}$ is in H_{1234} . Then $P_{12} Q_t P_{12}^{-1} = N - Q_t$, which justifies P_{12} as an antiunitary particle-hole transformation. And P_{12} also commutes with the Hamiltonian

$[P_{12}, H_{1234}] = 0$. It seems to indicate that the ELS is the same as the complex fermion SYK case discussed previously [21,22,27]: (i) If $N \pmod{4} = 1, 3$ it is GUE with $d_t = 1$ in a given parity Q_t ; (ii) if $N \pmod{4} = 0$, it is GOE with $d_t = 1$ in a given parity Q_t ; and (iii) If $N \pmod{4} = 2$, it is GSE with $d_t = 2$ in a given parity Q_t . Unfortunately, these results are inconsistent with those listed in Table III. In the following, we study how to remedy these problems.

1. N is even

Obviously, the total parity $Q_{12} = Q_1 + Q_2$ is not enough, because (Q_1, Q_2) are separately conserved. It may not be convenient to express (Q_1, Q_2) in terms of the complex fermions c_i, c_i^\dagger in this basis, but it can be most conveniently expressed in terms of the Majorana fermions, as shown below.

To fix this problem, we may still take $Q_1 = \sum_{i=1}^{N_c} c_{i1}^\dagger c_{i1} = \sum_{i=1}^{N_c} (\frac{1}{2} - i\chi_{1,2i} \chi_{1,2i-1})$, where $N_c = N/2$ as defined in Sec. III A. Note that in the intercolor scheme [Fig. 8(a)], Q_1 becomes complex but remains Hermitian, so its eigenvalue remains positive. This is the price one must pay in this intercolor representation, which makes the Hamiltonian real (namely, $[K, H] = 0$), but many other operators, such as Q_1 , are complex. Similar results hold for Q_2 . Then one can show that $P_{12} Q_1 P_{12}^{-1} = N_c - Q_1$ and $P_{12} Q_2 P_{12}^{-1} = N_c - Q_2$, which recovers $P_{12} Q_t P_{12}^{-1} = N - Q_t$. When $N \pmod{4} = 0$, P_{12} maps (Q_1, Q_2) to the same sector, $P_{12}^2 = 1$; it is in the GOE. When $N \pmod{4} = 2$, P_{12} maps (Q_1, Q_2) to $(Q_1 + 1, Q_2 + 1)$ with the same total parity; it is in the GUE with $d_t = 2$ in the total parity sector. So we have recovered the results listed in Table III for even N in this intercolor scheme.

Note that if one performs the exact diagonalization in the Q_{12} basis, then it mixes the two completely unrelated parity sectors (Q_1, Q_2) and $(Q_1 + 1, Q_2 + 1)$, so one will find that the ELS may be something similar to the Poisson statistics shown in Fig. 3(d). So, only when doing exact diagonalization in a given parity sector (Q_1, Q_2) will the ELS show its real face: the GOE.

In fact, there is a more straightforward way to perform the classification and also find the degeneracy. The parity of the number operator Q_a , $a = 1, 2$ can be written as $(-1)^{Q_a} = (i\chi_{a,1} \chi_{a,2})(i\chi_{a,3} \chi_{a,4}) \dots (i\chi_{a,N-1} \chi_{a,N})$. Because the color 1 $\chi_{1,i}$ is completely real and color 2 $\chi_{2,i}$ is completely imaginary, we have $K(-1)^{Q_a} K = i^{N/2} (-1)^{Q_a}$, $a = 1, 2$. When $N \pmod{4} = 0$, the antiunitary operator K keeps both parities and $K^2 = 1$, which tells us that the ESL is the GOE. However, when $N \pmod{4} = 2$, K maps (Q_1, Q_2) to $(Q_1 + 1, Q_2 + 1)$ with the same total parity. So it is in the GUE with $d_t = 2$ in the total parity sector Q_{12} .

2. N is odd

When N is odd, the exact diagonalization is most conveniently and economically done without adding any

Majorana fermions at ∞ . The classifications can be done either with or without adding. So the two theoretical approaches are complementary to each other and should lead to the same answers when the degeneracy is counted carefully and correctly.

a. Classification in the minimum Hilbert space without adding Majorana fermions at ∞

Even in this case, there is no need to add extra decoupled Majorana fermions at ∞ . Although Q_1, Q_2 makes no sense anymore, Q_{12} is still well defined, and one can perform the exact diagonalization in the minimal Hilbert space with just one conserved quantity Q_{12} . Because $(-1)^{Q_{12}} = (i\chi_{1,1}\chi_{2,1})(i\chi_{1,2}\chi_{2,2}) \cdots (i\chi_{1,N}\chi_{2,N})$ is always real, K keeps the parity and $K^2 = 1$, which tells us that the ESL is the GOE. Since $P_{12}Q_{12}P_{12}^{-1} = N - Q_t$, P_{12} maps Q_{12} to $Q_{12} + 1$, so $d_t = 1 + 1$.

b. Classification in the enlarged Hilbert space by adding Majorana fermions at ∞

In the following, we will perform the classification and also find the degeneracy in the enlarged Hilbert space by adding decoupled Majorana fermions at ∞ . In fact, as shown in Sec. 2 a above, this is not necessary in the intercolor scheme and in the balanced case. However, it is constructive to do it here to compare with the intracolor scheme used in the main text.

As shown in Sec. III B, one can add $\chi_{1,N+1} = \chi_{1\infty}$ and $\chi_{2,N+1} = \chi_{2\infty}$ to explicitly make the parity \tilde{Q}_1 conservation in color 1 and color 2, respectively. By adding the two Majorana fermions at ∞ , one doubles the Hilbert space and also generates one more conserved parity. In this intercolor scheme, it is convenient to take (Q_{12}, \tilde{Q}_{12}) as a complete set, where Q_{12} is the total parity without adding the two Majorana fermions, and $\tilde{Q}_{12} = Q_{12} + n_{12\infty}$ is the total parity including the two added Majorana fermions.

There are also two corresponding operators $P_{12}, P_{12}^2 = (-1)^{N_c-1}$ and $\tilde{P}_{12} = P_{12}\chi_{1\infty}, \tilde{P}_{12}^2 = (-1)^{N_c}$, where $N_c = (N+1)/2$ as defined in Sec. III B. One can work out how the two operators act on the two conserved quantities: $P_{12}Q_{12}P_{12}^{-1} = N - Q_{12}$, $P_{12}\tilde{Q}_{12}P_{12}^{-1} = N - \tilde{Q}_{12} + 2n_{12\infty}$ and $\tilde{P}_{12}Q_{12}\tilde{P}_{12}^{-1} = N - Q_{12}$, $\tilde{P}_{12}\tilde{Q}_{12}\tilde{P}_{12}^{-1} = N + 1 - \tilde{Q}_{12}$. Unfortunately, neither of the two keeps the parity (Q_{12}, \tilde{Q}_{12}) . One may try to use any combinations of P_{12}, \tilde{P}_{12} and R_{12}, \tilde{R}_{12} to construct relevant operators. For example, one can try $P = KP_{12}\tilde{P}_{12} = K\chi_{1\infty}$, but then $PQ_{12}P^{-1} = Q_{12}$, $P\tilde{Q}_{12}P^{-1} = 1 - \tilde{Q}_{12}$, so it still does not work. However, if one removes $\chi_{1\infty}$ from P , then just $K = P\chi_{1\infty}$ alone does the job. Because $K^2 = 1$, it is in the GOE.

In fact, more straightforwardly, because both $(-1)^{Q_{12}}$ and $(-1)^{\tilde{Q}_{12}}$ are real, K keeps both parities and $K^2 = 1$, which tells us that the ESL is the GOE.

Note also that \tilde{P}_{12} maps (Q_{12}, \tilde{Q}_{12}) to $(Q_{12} + 1, \tilde{Q}_{12})$, so $d = 1$ in the minimal Hilbert space with just one conserved quantity Q_{12} , but $d_t = 1 + 1$ in the enlarged Hilbert space with a given parity of \tilde{Q}_{12} , so it cannot be observed in the exact diagonalization performed in the minimal Hilbert space Q_{12} .

For N odd, using this intercolor (Q_{12}, \tilde{Q}_{12}) scheme, we recover the results in Table III achieved in the main text in the intracolor $(\tilde{Q}_1, \tilde{Q}_2)$ scheme.

APPENDIX B: FOUR-COLORED SYK MODELS: TENFOLD WAY AND OPERATOR P_{12} (P_{34}) ACROSS THE FIRST TWO (THE OTHER TWO) COLORS AND $P = KP_{12}P_{34}$.

Just like the two-colored SYK model discussed above, one can introduce N complex fermions from the first two colors $c_i = (\chi_{1i} - i\chi_{2i})/\sqrt{2}$, $c_i^\dagger = (\chi_{1i} + i\chi_{2i})/\sqrt{2}$ and their number operator $Q_c = \sum_i c_i^\dagger c_i$. One defines the antiunitary particle-hole symmetry operator to be $P_{12} = K \prod_{i=1}^N (c_i^\dagger + c_i)$. In fact, $R_{12} = K \prod_{i=1}^N (c_i^\dagger - c_i)$ works equally well, but it will not lead to new symmetry. It is easy to show that $P_{12}^2 = (-1)^{\lfloor N/2 \rfloor}$. One can also show that $P_{12}c_i P_{12} = \eta c_i^\dagger$, $P_{12}c_i^\dagger P_{12} = \eta c_i$, and $P_{12}\chi_{ai} P_{12} = \eta\chi_{ai}$, $a = 1, 2$, where $\eta = (-1)^{\lfloor (N-1)/2 \rfloor}$.

One can also introduce N complex fermions from the other two colors $d_i = (\chi_{3i} - i\chi_{4i})/\sqrt{2}$, $d_i^\dagger = (\chi_{3i} + i\chi_{4i})/\sqrt{2}$ and their number operator $Q_d = \sum_i d_i^\dagger d_i$. One can also define the similar antiunitary operator P_{34} (or R_{34}). It is easy to see that P_{34} or R_{34} can do the same job, but they cannot provide new information. Of course, one can group them differently such as P_{13}, P_{24} or P_{14}, P_{23} , and they should lead to the same answers.

It can be shown that P_{12} (also P_{34}) anticommutes with the Hamiltonian $\{P_{12}, H_{1234}\} = 0$. The total number of fermions $Q_t = \sum_i (c_i^\dagger c_i + d_i^\dagger d_i) = Q_c + Q_d$ is not a conserved quantity, but its parity $(-1)^{Q_t}$ is. In fact, the parities $(-1)^{Q_c}$ and $(-1)^{Q_d}$ are separately conserved. We have $P_{12}Q_c P_{12}^{-1} = N - Q_c$, $P_{12}Q_d P_{12}^{-1} = Q_d$, so it maps to the same (opposite) parity in the Q_c sector when N is even (odd). Similarly, $P_{34}Q_c P_{34}^{-1} = Q_c$ and $P_{34}Q_d P_{34}^{-1} = N - Q_d$.

One can also define another antiunitary operator as

$$P = K \prod_{i=1}^N (c_i^\dagger + c_i)(d_i^\dagger + d_i) = P_{12}P_{34}K, \quad (\text{B1})$$

which can be contrasted with the similar operator in the two-colored case [Eq. (8)]. It is easy to show that $P^2 = (-1)^N$ and $[P, H_{1234}] = 0$. It is also easy to see that $PQ_c P^{-1} = N - Q_c$ and $PQ_d P^{-1} = N - Q_d$. Then $PQ_t P^{-1} = N - Q_c + N - Q_d = 2N - Q_t$, so it always maps to the same total parity.

1. N is even

When combining P with $P^2 = (-1)^N$ and P_{12} with $P_{12}^2 = (-1)^{\lfloor N/2 \rfloor}$, paying special attention to their action on the Hilbert space with given parities in $(-1)^{Q_c}$ and $(-1)^{Q_d}$, one can see that when $N \pmod{4} = 0, 2$, (Q_c, Q_d) maps to the same sector, so H_{1234} belongs to class BDI (chGOE) or class CI (BdG), respectively. The degeneracy $d = 1$. These facts completely agree with the $N \pmod{4} = 0, 2$ case listed in Table IV. Note that one can also combine P in Eq. (B1) with any other P_{ij} or R_{ij} without affecting the results [71]. Namely, one needs to pick up just one representation, (P, P_{ij}) or (P, R_{ij}) .

As alerted earlier, one can introduce N complex fermions from colors 2 and 3, with $f_i = (\chi_{3i} - i\chi_{2i})/\sqrt{2}$, $f_i^\dagger = (\chi_{3i} + i\chi_{2i})/\sqrt{2}$ and their number operator $Q_{23} = Q_f = \sum_i f_i^\dagger f_i$. One can also define the similar antiunitary operator P_{23} (or R_{23}). Of course, Q_{23} enclosed in the box in Fig. 9(a) is also a conserved parity. When N is even, it also commutes with (Q_{12}, Q_{34}) . Although it may not be conveniently expressed in terms of the two groups of complex fermions c_i and d_i , they can be conveniently expressed in terms of Majorana fermions of colors 2 and 3. One can show that acting on them with P and P_{12} does not affect the results above achieved with (Q_{12}, Q_{34}) only.

Now we find two antiunitary operators, one commuting and another anticommuting with H_{1234} . From the two antiunitary operators, one can define the chirality operator $\Lambda = P_{12}P = P_{34}K = \chi_{3,1}\chi_{3,2}\cdots\chi_{3,N}$, which is nothing but proportional to the parity operator $i^{-N/2}(-1)^{Q_3}$ of the color 3. It is a unitary operator anticommuting with the Hamiltonian $\{\Lambda, H_{1234}\} = 0$ and also keeps all the parities (Q_{12}, Q_{23}, Q_{34}) . Of course, $\Lambda = P_{12}K = \chi_{1,1}\chi_{1,2}\cdots\chi_{1,N} = i^{-N/2}(-1)^{Q_1}$ works equally well as the unitary chirality operator.

In fact, there is a more straightforward way to do the classification and also find the degeneracy. Because all three parities (Q_{12}, Q_{23}, Q_{34}) are real, $T_+ = K$ keeps them all, and $K^2 = 1$. Because the Hamiltonian is real, $[K, H] = 0$. Note that we also have the chiral (mirror) symmetry $\{(-1)^{Q_a}, H\} = 0$, where $(-1)^{Q_a} = (i\chi_{a,1}\chi_{a,2}\cdots i\chi_{a,N-1}\chi_{a,N})$ and $a = 1, 2, 3, 4$. Thus, we can construct the other antiunitary operator as $T_- = K(-1)^{Q_a}$, which anticommutes with the Hamiltonian. From the fact that $\{(-1)^{Q_a}, (-1)^{Q_b}\} = 0$, one can see that T_- keeps all three parities. Since $(-1)^{Q_a}$ has the same sign as $i^{N/2}$, it is easy to see that $T_-^2 = (-1)^{N/2}$. Combining $T_+ = K$, $T_+^2 = 1$ and $T_- = K(-1)^{Q_a}$, $T_-^2 = (-1)^{N/2}$, we conclude that when $N \pmod{4} = 0$, it is class BDI, and when $N \pmod{4} = 2$, it is class CI.

2. N is odd

Similarly to the two-colored case, when N is odd, the exact diagonalization is most conveniently and economically done without adding any Majorana fermions at ∞ .

The classifications can be performed either with or without adding, so the two theoretical approaches are complementary to each other and should lead to the same answers.

a. Classification in the minimum Hilbert space without adding Majorana fermions at ∞

Even in this case, there is no need to add extra Majorana fermions at ∞ . There are still three conserved quantities Q_{12}, Q_{23}, Q_{34} , but Q_{23} does not commute with (Q_{12}, Q_{34}) anymore, so we still perform the exact diagonalization in the minimal Hilbert space with just two conserved quantities (Q_{12}, Q_{34}) . Because both Q_{12} and Q_{34} are real, the complex conjugate K holds for (Q_{12}, Q_{34}) and $K^2 = 1$. Again, the Hamiltonian is real, so $[K, H] = 0$. These facts tell us that the ESL is the GOE. Note that $(-1)^{Q_a}$ is not defined for odd N . As said above, P maps (Q_{12}, Q_{34}) to $(Q_{12} + 1, Q_{34} + 1)$, so the level degeneracy is $d = 1$ in the minimum Hilbert space with given (Q_{12}, Q_{34}) , and the level degeneracy is $d_t = 2$ in the total parity sector $Q_t = Q_{12} + Q_{34}$. This $d_t = 2$ can be seen in the exact diagonalization in a given total parity Q_t . These results recover those listed in Table IV.

b. Classification in the enlarged Hilbert space by adding Majorana fermions at ∞

In the following, we will perform the classification and also find the degeneracy in the enlarged Hilbert space by adding decoupled Majorana fermions at infinity. In fact, as shown in Sec. 2 a above, this is not necessary in the intercolor scheme and in the balanced case. However, it is constructive to do it here to compare with the scheme used in the main text.

As shown in Sec. V B, one can add $\chi_{a,N+1} = \chi_{a\infty}$, $a = 1, 2, 3, 4$ to make the parity conservation in $(\tilde{Q}_{12}, \tilde{Q}_{23}, \tilde{Q}_{34}, Q_t)$ explicitly [72]. Then one can repeat the procedures as in the N -even case in Sec. I above with $N \rightarrow N + 1$. In this intercolor scheme, it is more convenient to take $(\tilde{Q}_{12}, Q_{12}, \tilde{Q}_{34}, Q_{34})$ as the complete set, which is complementary to the set $(\tilde{Q}_{12}, \tilde{Q}_{23}, \tilde{Q}_{34}, Q_t)$ used in the main text [72]. In this set, (Q_{12}, Q_{34}) is the parity without adding the four Majorana fermions [enclosed in the two boxes in Fig. 9(b)], and $\tilde{Q}_{12} = Q_{12} + n_{12\infty}$, $\tilde{Q}_{34} = Q_{34} + n_{34\infty}$ is the parity including the four Majorana fermions. One can also construct two new operators $\tilde{P}_{12} = P_{12}\chi_{1\infty}$ and $\tilde{P}_{34} = P_{34}\chi_{3\infty}$ with $\tilde{P}_{12}^2 = \tilde{P}_{34}^2 = (-1)^{\lfloor (N+1)/2 \rfloor}$. They lead to a new composite operator $\tilde{P} = K\tilde{P}_{12}\tilde{P}_{34}$ with $\tilde{P}^2 = (-1)^{N+1} = 1$.

Unfortunately, similarly to the two-colored case discussed above, none of these operators keep the complete set of the parities $(Q_{12}, \tilde{Q}_{12}, Q_{34}, \tilde{Q}_{34})$ in the same sector. One can try to use $P_{12}, \tilde{P}_{12}, R_{12}, \tilde{R}_{12}$ for colors 1 and 2, and $P_{34}, \tilde{P}_{34}, R_{34}, \tilde{R}_{34}$ for colors 3 and 4 to construct relevant operators in this intercolor scheme.

Taking the experience from the two-colored case, it turns out that just K alone does the job. Because $K^2 = 1$, it is in the GOE.

In fact, more straightforwardly, since all four parities of $(Q_{12}, \tilde{Q}_{12}, Q_{34}, \tilde{Q}_{34})$ are real, K keeps all the parities and $K^2 = 1$ which tells us the ESL is the GOE. Of course, all four colors' individual parities still anticommute with the Hamiltonian $\{(-1)^{\tilde{Q}_a}, H\} = 0$, $i = 1, 2, 3, 4$, but none can keep all the cross parities. For example, $(-1)^{\tilde{Q}_1}$ keeps \tilde{Q}_{12} but changes Q_{12} . Note that $(-1)^{\tilde{Q}_a}$ is not a chiral operator for odd N .

Note also that \tilde{P} maps $(Q_{12}, Q_{34}, \tilde{Q}_{12}, \tilde{Q}_{34})$ to $(Q_{12} + 1, Q_{34} + 1, \tilde{Q}_{12}, \tilde{Q}_{34})$, which has the same total parity $Q_t = Q_{12} + Q_{34}$, so $d = 1$ at a given parity (Q_{12}, Q_{34}) and $d_t = 2$ with the total parity Q_t , consistent with that listed for $N \pmod{4} = 1, 3$ in Table IV. Obviously, this double degeneracy can be observed in the exact diagonalization performed in the total parity Q_t sector shown in Figs. 7(a) and 7(c). Of course, this scheme cannot even be used in the imbalanced case.

Finally, we conclude that the biggest advantage to using the intercolor scheme is that the Hamiltonian is made real: if all the conserved quantities are real, then the bulk ESL must be the GOE. This is why seven out of eight cases in Tables III and IV are real. The only exception is that in the two-colored case with $N \pmod{4} = 2$, as shown in Sec. I of Appendix A, both Q_1 and Q_2 are imaginary, so it is in the GUE. As is shown in Refs. [35–39] in the Dicke model, K is the only relevant antiunitary operator which commutes with the Dicke Hamiltonian, so $K^2 = 1$ only leads to the GOE for the Dicke model.

Unfortunately, as said before, this intercolor scheme cannot be extended to the imbalanced case. When

generalizing the method used in the main text to all the possible imbalanced cases with $q = 4$, we find all ten classes in the tenfold classifications [70].

APPENDIX C: CLASSIFICATIONS OF THE HYBRID TWO- AND FOUR-COLORED SYK MODELS IN THE INTERCOLOR SCHEME

It turns out that the intercolor scheme may be used to reach the classifications of the hybrid two- and four-colored SYK models more quickly than the intracolor scheme used in the main text. The complex conjugate operator K is the operator that does most of the job.

1. Hybrid two-colored case

For the representation used in Fig. 8, the hybrid Hamiltonian H_{1122}^{Hb} in Eq. (12) is real, and the only conserved quantity is total parity $(-1)^{Q_t}$. No matter if N is even or odd, $Q_t = Q_{12}$ is always real, and thus $(-1)^{Q_t}$ is also real. Then $[K, H_{1122}^{Hb}] = 0$ and $[K, (-1)^{Q_t}] = 0$. Of course, $K^2 = 1$, so its ESL is the GOE at any ratio J/K .

2. Hybrid four-colored case

Since the quadratic term $i \sum_{i,j,a<b} K_{ij}^{ab} \chi_{ai} \chi_{bj}$ contains all kinds of intercolor couplings, the intercolor scheme shown in Fig. 9 cannot be used to make it real. In fact, it has no symmetry, so the ESL of the total Hamiltonian H_{1234}^{Hb} in Eq. (27) is in the GUE at $J/K \sim 1$. If one changes the quadratic term to $i \sum K_{ij} (\chi_{1i} \chi_{2j} + \chi_{3i} \chi_{4j})$, then just like the hybrid two-colored case, it also becomes real; the modified hybrid four-colored SYK model must also be in the GOE at $J/K \sim 1$.

-
- [1] M. Z. Hasan and C. L. Kane, Colloquium: Topological insulators, *Rev. Mod. Phys.* **82**, 3045 (2010).
 - [2] X. L. Qi and S. C. Zhang, Topological insulators and superconductors, *Rev. Mod. Phys.* **83**, 1057 (2011).
 - [3] C.-K. Chiu, J. C. Y. Teo, A. P. Schnyder, and S. Ryu, Classification of topological quantum matter with symmetries, *Rev. Mod. Phys.* **88**, 035005 (2016).
 - [4] X.-G. Wen, Colloquium: Zoo of quantum-topological phases of matter, *Rev. Mod. Phys.* **89**, 041004 (2017).
 - [5] S. Sachdev and J. Ye, Gapless Spin Liquid Ground State in a Random Quantum Heisenberg Magnet, *Phys. Rev. Lett.* **70**, 3339 (1993).
 - [6] A. Georges, O. Parcollet, and S. Sachdev, Quantum fluctuations of a nearly critical Heisenberg spin glass, *Phys. Rev. B* **63**, 134406 (2001).
 - [7] A. Y. Kitaev, A simple model of quantum holography, KITP Program: Entanglement in Strongly-Correlated Quantum Matter (2015), <http://online.kitp.ucsb.edu/online/entangled15/kitaev/>, <http://online.kitp.ucsb.edu/online/entangled15/kitaev2/>.
 - [8] S. Sachdev, Bekenstein-Hawking Entropy and Strange Metals, *Phys. Rev. X* **5**, 041025 (2015).
 - [9] J. Ye, Two indices Sachdev-Ye-Kitaev model, arXiv: 1809.0667, substantially revised second version to be put on arXiv soon.
 - [10] J. Polchinski and V. Rosenhaus, The spectrum in the Sachdev-Ye-Kitaev model, *J. High Energy Phys.* **04** (2016) 001.
 - [11] J. Maldacena and D. Stanford, Remarks on the Sachdev-Ye-Kitaev model, *Phys. Rev. D* **94**, 106002 (2016).
 - [12] D. J. Gross and V. Rosenhaus, A Generalization of Sachdev-Ye-Kitaev, *J. High Energy Phys.* **02** (2017) 093.
 - [13] D. Bagrets, A. Altland, and A. Kamenev, Sachdev-Ye-Kitaev model as Liouville quantum mechanics, *Nucl. Phys.* **B911**, 191 (2016).

- [14] T. G. Mertens, G. J. Turiaci, and H. L. Verlinde, Solving the Schwarzian via the conformal bootstrap, *J. High Energy Phys.* **08** (2017) 136.
- [15] D. Stanford and E. Witten, Fermionic localization of the Schwarzian theory, *J. High Energy Phys.* **10** (2017) 008.
- [16] A. Kitaev and S. J. Suh, The soft mode in the Sachdev-Ye-Kitaev model and its gravity dual, *J. High Energy Phys.* **05** (2018) 183.
- [17] V. Rosenhaus, An introduction to the SYK model, *J. Phys. A: Math. Theor.* **52**, 323001 (2019).
- [18] J. Maldacena, S. H. Shenker, and D. Stanford, A bound on chaos, *J. High Energy Phys.* **08** (2016) 106.
- [19] J. Maldacena, D. Stanford, and Z. Yang, Conformal symmetry and its breaking in two dimensional nearly anti-de Sitter space, *Prog. Theor. Exp. Phys.* **2016**, 12C104 (2016).
- [20] A. Kitaev and S. J. Suh, Statistical mechanics of a two-dimensional black hole, *J. High Energy Phys.* **05** (2019) 198.
- [21] W. Fu and S. Sachdev, Numerical study of fermion and boson models with infinite-range random interactions, *Phys. Rev. B* **94**, 035135 (2016).
- [22] Y.-Z. You, A. W. W. Ludwig, and C. Xu, Sachdev-Ye-Kitaev model and thermalization on the boundary of many-body localized Fermionic symmetry protected topological states, *Phys. Rev. B* **95**, 115150 (2017).
- [23] J. S. Cotler, G. Gur-Ari, M. Hanada, J. Polchinski, P. Saad, S. H. Shenker, D. Stanford, A. Streicher, and M. Tezuka, Black holes and random matrices, *J. High Energy Phys.* **05** (2017) 118.
- [24] A. M. Garc a-Garc a and J. J. M. Verbaarschot, Spectral and thermodynamic properties of the Sachdev-Ye-Kitaev model, *Phys. Rev. D* **94**, 126010 (2016).
- [25] T. Li, J. Liu, Y. Xin, and Y. Zhou, Supersymmetric SYK model and random matrix theory, *J. High Energy Phys.* **06** (2017) 111.
- [26] T. Kanazawa, Tilo Wettig and Complete random matrix classification of SYK models with $\mathcal{N} = 0, 1$ and 2 supersymmetry, *J. High Energy Phys.* **09** (2017) 050.
- [27] Y. Yi-Xiang, F. Sun, J. Ye, and W.-M. Liu, A new universal ratio in random matrix theory and quantum analog of Kolmogorov-Arnold-Moser theorem in Type-I and Type-II hybrid Sachdev-Ye-Kitaev models, [arXiv:1809.07577](https://arxiv.org/abs/1809.07577).
- [28] R. Gurau, The complete $1/N$ expansion of a SYK-like tensor model, *J. Nucl. Phys. B* **916**, 386 (2017).
- [29] E. Witten, An SYK-like model without disorder, [arXiv:1610.09758](https://arxiv.org/abs/1610.09758).
- [30] I. R. Klebanov and G. Tarnopolsky, Uncolored random tensors, melon diagrams, and the SYK models, *Phys. Rev. D* **95**, 046004 (2017).
- [31] V. Bonzom, L. Lionni, and A. Tanasa, Diagrammatics of a colored SYK model and of an SYK-like tensor model, leading and next-to-leading orders, *J. Math. Phys. (N.Y.)* **58**, 052301 (2017).
- [32] K. Bulychева, I. R. Klebanov, A. Milekhin, and G. Tarnopolsky, Spectra of operators in large N tensor models, *Phys. Rev. D* **97**, 026016 (2018).
- [33] I. R. Klebanov, F. Popov, and G. Tarnopolsky, TASI lectures on large N tensor models, *Proc. Sci., TASI2017* (2018) 004 [[arXiv:1808.09434](https://arxiv.org/abs/1808.09434)].
- [34] The history of the colored SYK versus SYK is just opposite to that of the colored tensor versus uncolored tensor model. Gross and Rosenhaus [12] put colors on the original SYK model, while Klebanov and Tarnopolsky [30] uncolored the original colored tensor (Gurau-Witten) model.
- [35] Y. Yi-Xiang, J. Ye, and C. Zhang, Photon Berry phases, instantons, quantum chaos and quantum analog of Kolmogorov-Arnold-Moser theorem in the $U(1)/Z_2$ Dicke models, [arXiv:1903.02947](https://arxiv.org/abs/1903.02947).
- [36] J. Ye and C. Zhang, Super-radiance, photon condensation and its phase diffusion, *Phys. Rev. A* **84**, 023840 (2011).
- [37] Y. Yi-Xiang, J. Ye, and W. M. Liu, Goldstone and Higgs modes of photons inside a cavity, *Sci. Rep.* **3**, 3476 (2013).
- [38] Y. Yi-Xiang, J. Ye, W. M. Liu, and C. Zhang, Comments on ‘‘Controlling Discrete and Continuous Symmetries in Super-radiant Phase Transitions with Circuit QED Systems,’’ [arXiv:1506.06382](https://arxiv.org/abs/1506.06382).
- [39] Y. Yi-Xiang, J. Ye, and C. Zhang, Parity oscillations and photon correlation functions in the $Z_2/U(1)$ Dicke model at a finite number of atoms or qubits, *Phys. Rev. A* **94**, 023830 (2016).
- [40] Y. Y. Atas, E. Bogomolny, O. Giraud, and G. Roux, Distribution of the Ratio of Consecutive Level Spacings in Random Matrix Ensembles, *Phys. Rev. Lett.* **110**, 084101 (2013).
- [41] The simplest case is the $N \pmod{8} = 0$ case in the SYK, $P^2 = 1$; it also maps Q to the same sector, so it is in the GOE with $d = 1$ at a given parity Q . However, there is another parity sector, and the two parity sectors are completely uncorrelated, so it is not known which parity sector contains the ground state. However, if performing exact diagonalization in both parity sectors, one gets something similar to the Poisson. The rigorous RMT of this mixed two uncorrelated random matrix ensemble was presented in Sec. II B. See also Appendix A.
- [42] Y. Y. Atas, E. Bogomolny, O. Giraud, P. Vivo, and E. Vivo, Joint probability densities of level spacing ratios in random matrices, *J. Phys. A* **46**, 355204 (2013).
- [43] This is similar to the $N \pmod{8} = 6$ case in the SYK, $P^2 = -1$; it also maps Q to the opposite sector $Q + 1$, so it is in the GUE with $d = 1$ at a given parity Q . However, it has the $d_t = 2$ double degeneracy when considering both parity sectors. See also Appendix A.
- [44] L. Fidkowski and A. Kitaev, Topological phases of fermions in one dimension, *Phys. Rev. B* **83**, 075103 (2011).
- [45] I. Kourkoulou and J. Maldacena, Pure states in the SYK model and nearly-AdS₂ gravity, [arXiv:1707.02325](https://arxiv.org/abs/1707.02325).
- [46] Of course and in the $q = 4$ case, one can equally use the P_m operator (plus P_z) to characterize the symmetry of H_4 and reach the same conclusion as that from using P (plus P_z).
- [47] A. Altland and M. R. Zirnbauer, Nonstandard symmetry classes in mesoscopic normal-superconducting hybrid structures, *Phys. Rev. B* **55**, 1142 (1997).
- [48] A. Altland and M. R. Zirnbauer, Random Matrix Theory of a Chaotic Andreev Quantum Dot, *Phys. Rev. Lett.* **76**, 3420 (1996).
- [49] L. Balents, L. Bartosch, A. Burkov, S. Sachdev, and K. Sengupta, Putting competing orders in their place near the Mott transition, *Phys. Rev. B* **71**, 144508 (2005).

- [50] J. Ye, Duality, Magnetic space group and their applications to quantum phases and phase transitions on bipartite lattices in several experimental systems, *Nucl. Phys.* **B805**, 418 (2008).
- [51] Y. Chen and J. Ye, Characterizing boson orders in lattices by vortex degree of freedoms, *Philos. Mag.* **92**, 4484 (2012).
- [52] J. Ye and C. Yan, Quantum phases, supersolids and quantum phase transitions of interacting bosons in frustrated lattices, *Nucl. Phys.* **B869**, 242 (2013).
- [53] A. Vishwanath and T. Senthil, Physics of Three-Dimensional Bosonic Topological Insulators: Surface-Deconfined Criticality and Quantized Magnetoelectric Effect, *Phys. Rev. X* **3**, 011016 (2013).
- [54] J. Yoon, SYK models and SYK-like tensor models with global symmetry, *J. High Energy Phys.* **10** (2017) 183.
- [55] E. P. Wigner, On the statistical distribution of the widths and spacings of nuclear resonance levels, *Proc. Cambridge Philos. Soc.* **47**, 790 (1951).
- [56] F. Dyson, Statistical theory of the energy levels of complex systems: I, *J. Math. Phys. (N.Y.)* **3**, 140 (1962).
- [57] K. Efetov, *Supersymmetry in Disorder and Chaos* (Cambridge University Press, Cambridge, England, 1996).
- [58] E. V. Shuryak and J. J. M. Verbaarschot, Random matrix theory and spectral sum rules for the Dirac operator in QCD, *Nucl. Phys.* **A560**, 306 (1993).
- [59] J. J. M. Verbaarschot, Spectrum of the QCD Dirac Operator and Chiral Random Matrix Theory, *Phys. Rev. Lett.* **72**, 2531 (1994).
- [60] T. Kanazawa and T. Wettig, Stressed Cooper pairing in QCD at high isospin density: Effective Lagrangian and random matrix theory, *J. High Energy Phys.* **10** (2014) 55.
- [61] T. Kanazawa, T. Wettig, and N. Yamamoto, Banks-Casher-type relation for the BCS gap at high density, *Eur. Phys. J. A* **49**, 88 (2013).
- [62] V. J. Emery and S. Kivelson, Mapping of the two-channel Kondo problem to a resonant-level model, *Phys. Rev. B* **46**, 10812 (1992).
- [63] J. M. Maldacena and A. W. W. Ludwig, Majorana fermions, exact mapping between quantum impurity fixed points with four bulk Fermion species, and solution of the “unitarity puzzle,” *Nucl. Phys.* **B506**, 565 (1997).
- [64] J. Ye, Emery-Kivelson Line and Universality of Wilson Ratio of Spin Anisotropic Kondo Model, *Phys. Rev. Lett.* **77**, 3224 (1996).
- [65] J. Ye, Abelian Bosonization Approach to Quantum Impurity Problems, *Phys. Rev. Lett.* **79**, 1385 (1997).
- [66] I. Danshita, M. Hanada, and M. Tezuka, Creating and probing the Sachdev-Ye-Kitaev model with ultracold gases: Towards experimental studies of quantum gravity, *Prog. Theor. Exp. Phys.* **2017**, 083I01 (2017).
- [67] D. I. Pikulin and M. Franz, Black Hole on a Chip: Proposal for a Physical Realization of the Sachdev-Ye-Kitaev Model in a Solid-State System, *Phys. Rev. X* **7**, 031006 (2017).
- [68] A. Chew, A. Essin, and J. Alicea, Approximating the Sachdev-Ye-Kitaev model with Majorana wires, *Phys. Rev. B* **96**, 121119 (2017).
- [69] L. García-Álvarez, I. L. Egusquiza, L. Lamata, A. del Campo, J. Sonner, and E. Solano, Digital Quantum Simulation of Minimal AdS/CFT, *Phys. Rev. Lett.* **119**, 040501 (2017).
- [70] F. Sun and J. Ye, Random matrix theory and $1/N$ expansion of quantum chaos in strongly correlated warmholes (unpublished).
- [71] To some extent and this is similar to the case of the central potential quantum mechanical problem—one can choose the complete set J^2, J_z or J^2, J_x or J^2, J_y , but $J_i, i = x, y, z$ do not commute with each other.
- [72] Note that due to adding Majorana fermions at ∞ , there is a shift of notation here from the main text to the two appendixes when N is odd in the two-color case. We change from (Q_1, Q_2) in the main text to $(\tilde{Q}_1, \tilde{Q}_2)$ in Appendix A. In the four-color case, $(Q_{12}, Q_{23}, Q_{34}, Q_{0t})$ is used in the main text, while $(\tilde{Q}_{12}, \tilde{Q}_{23}, \tilde{Q}_{34}, Q_t)$ is used in Appendix B.